The Pennsylvania State University

The Graduate School

Department of Electrical Engineering

AN ULTRASONIC GUIDED WAVE INSPECTION SYSTEM FOR HARD TO ACCESS CIVIL STRUCTURES

A Thesis in

Electrical Engineering

by

Siddharth Kishin Advani

Submitted in Partial Fulfillment
of the Requirements
for the Degree of

Master of Science

December 2009

The thesis of Siddharth Kishin Advani was reviewed and approved* by the following:

Joseph Rose
Paul Morrow Professor of Engineering Science and Mechanics
Thesis Co-Advisor

Qiming Zhang
Distinguished Professor of Electrical Engineering
Thesis Co-Advisor

Srinivas Tadigadapa
Associate Professor of Electrical Engineering

Ken Jenkins
Professor of Electrical Engineering
Head of the Department of Electrical Engineering

*Signatures are on file in the Graduate School

ABSTRACT

An ultrasonic guided wave inspection method is developed for the non-destructive evaluation (NDE) of hard to access isotropic plate-like structures. Experiments using Lamb waves and Shear Horizontal (SH) waves are conducted to determine the type of wave that will give maximum penetration power. Lamb waves are excited with an angle-wedge transducer and SH waves are generated using Electromagnetic Acoustic Transducers (EMATS). Results from these experiments are used to select the appropriate transducer at the correct operating frequency. Various tests are then carried out on buried plate-like structures having different anomaly geometries. Another significant objective of this work is to demonstrate the effectiveness of using wave propagation finite element methods to interrogate the possibility of estimating thinning loss due to corrosion in plates. A parametric study is carried out on two dimensional corrosion type surface breaking defects using Lamb waves. Based on this study, a method to solve the inverse problem of estimating the average thickness of an area being inspected is suggested.

TABLE OF CONTENTS

LIST OF FIGURES

LIST OF TABLES

ACKNOWLEDGEMENTS

I take this opportunity to express my sincere thanks to a number of people who have showed immense faith in my ability to complete this work successfully.

To my family, who have always been there for me. Their unconditional love and unfailing encouragement has been a source of great inspiration for me. I will never be able to thank them enough for their support.

To my advisor, Dr. Joseph L. Rose, whose immense wisdom has been the guiding light in my research for this work. As a part of Dr. Rose's research group, I have been provided with ample opportunities to expand my horizons and gain the knowledge and experience that I will need in the course of my career.

To my committee co-chair Dr. Qiming Zhang and committee member Dr. Srinivas Tadigadapa, for their valuable contributions to my work. Their advice, guidance and review have lent a new dimension to my understanding of this work.

To FBS, Inc., for providing excellent facilities that enabled timely completion of this project.

A special thanks to Ron Then and Richard Love for their assistance on the concrete experiment and Dr. Jason Van Velsor for his valuable insights.

CHAPTER 1

INTRODUCTION

Ultrasonic waves in solid media have now become a well established research area in the field of non-destructive evaluation (NDE). Ultrasonic NDE uses high-frequency elastic waves to evaluate components without affecting their integrity or performance. Most work so far in ultrasonic NDE has focused on the use of bulk waves to detect damages and anomalies such as cracks, corrosion and material degradation. However, ultrasonic guided wave inspection has expanded rapidly in many different areas of manufacturing and in-service inspection. The major difference between bulk wave propagation and guided wave propagation is that the former refers to wave propagation in either a half space or infinite space with no boundary disturbances and the later requires a boundary for their existence, for example wave propagation in a plate.

1.1 Objective

In some NDE applications, it is required to make thickness estimates of large plate-like civil structures. The traditional bulk wave thickness estimation technique is capable of providing information local to the area being inspected. Thus using the bulk wave thickness measurement technique to inspect a large structure on a point-by-point basis becomes very time consuming and increases labor costs. More importantly, point-

by-point inspection is not feasible in hidden or inaccessible structures like buried pipelines or pressure vessels. The guided wave technique allows inspection over long distances from a single pair of access points or even from only one access point. The purpose of this work is to tackle the problem of inspecting inaccessible plate-like structures with ultrasonic guided waves, using a systematic approach.

1.2 Preview of Work

Chapter 2 presents a concise literature review, which provided a strong foundation in developing the work contained herein.

Chapter 3 defines the problem and statement of work. Descriptions and photographs of the prototype model used for further analysis are provided.

Chapter 4 deals with penetration power studies for both Lamb wave and Shear Horizontal waves. Based on these results, the appropriate type of transducer and frequency of operation are suggested.

Chapter 5 delves into the beam spreading phenomenon of the Electromagnetic Acoustic Transducer (EMAT) used for generating SH waves. Based on various experiments, the sensitivity of the given EMAT to different anomalies under different conditions is predicted.

Chapter 6 describes a technique to estimate average thickness of the structure between two access points when looking at small gradual thinning type damages. This chapter introduces finite-element methods for developing this technique. A parametric study is carried out on two dimensional corrosion type surface breaking defects using Lamb waves. Based on this study, a method to solve the inverse problem of estimating average thickness of area being inspected is suggested.

Finally, Chapter 7 provides a concise summary of the important results presented within this thesis. Recommendations for future research are included in this chapter.

CHAPTER 2

LITERATURE REVIEW

This work has been built on a foundation that was laid down by many hallmark papers and famous works in the field of wave propagation. However, only a detailed review of the recent accomplishments in the area related to this work is provided. For a thorough review on wave propagation in solid media, one is pointed to [Graff 1975] and [Rose 1999].

2.1 Guided Waves in Plates

A complete range of techniques used in the field of non-destructive evaluation (NDE) is presented in [Achenbach 2000]. Ultrasonic techniques, however, remain at the helm of affairs. [Silk 1984] and [Krautkrämer and Krautkrämer 1990] describe the different methods available for the generation of ultrasound, with particular reference to nondestructive testing (NDT).

Over the past few years, the ultrasonic guided wave technique has begun to show its true capabilities with increasing technology transfer from different areas and advancing computational capabilities. [Rose 2000] and [Rose 2002] provide an extensive review of the applications of ultrasonic guided waves in the field of NDE.

A tremendous amount of work has already been done with regards to guided waves inspection in plate-like structures. [Fortunko *et al* 1982] looked at planar defects in plates using the low-frequency Shear Horizontal waves. [Cawley and Alleyne 1996] discussed the use of Lamb waves for long range inspection of plates. Defect characterization using both Lamb and SH-waves in a plate was studied by [Zhao 2003].

2.2 Related Work

[Rose *et al* 1994] demonstrated the ability of ultrasonic guided waves in finding defects in tubes that were not easily and efficiently detected by other means. [Pavlakovic *et al* 2001] looked at a case of a steel bar imbedded in grout for the purpose of detecting the onset of corrosion in the tendons in post-tensioned concrete bridges. [Rose 2003] showed how mode and frequency control play an important role in testing water loaded structures.

[Zhu *et al* 1998] used Boundary Element Method (BEM) to study the implications of corrosion type thinning on mode cutoff, group velocity, and transmission and reflection amplitudes. [Jenot *et al* 2001] used Lamb wave group velocity measurements and wavelet signal processing for corrosion thickness gauging in plates. [Luo and Rose 2003] used SH-Wave EMATs to develop a direct and an indirect measurement method based on the relationship between peak frequency shift and thickness changes in a stainless steel plate.

[Luo and Rose 2004] showed that even peak frequency shifts can be used to estimate thicknesses in plates using Lamb waves. [Breon 2008] referred to the above techniques to explore their effectiveness on non-uniform thickness changes of an isotropic plate-like structure using Lamb type waves. [Jenot *et al* 2007] used guided wave propagation FEM techniques to look at linear variations of plate thickness.

CHAPTER 3

PROBLEM DEFINITION AND THE GUIDED WAVE METHOD

3.1 Problem Statement

There are many plate-like structures that exhibit limited accessibility over a large area. Examples of such structures are the lining of a nuclear reactor, an underground tunnel, a liquid-filled storage tank etc. Such structures are difficult to inspect using the traditional bulk wave methodology. Guided waves can offer an efficient solution for the inspection of such structures as shown in Figure 3.1.

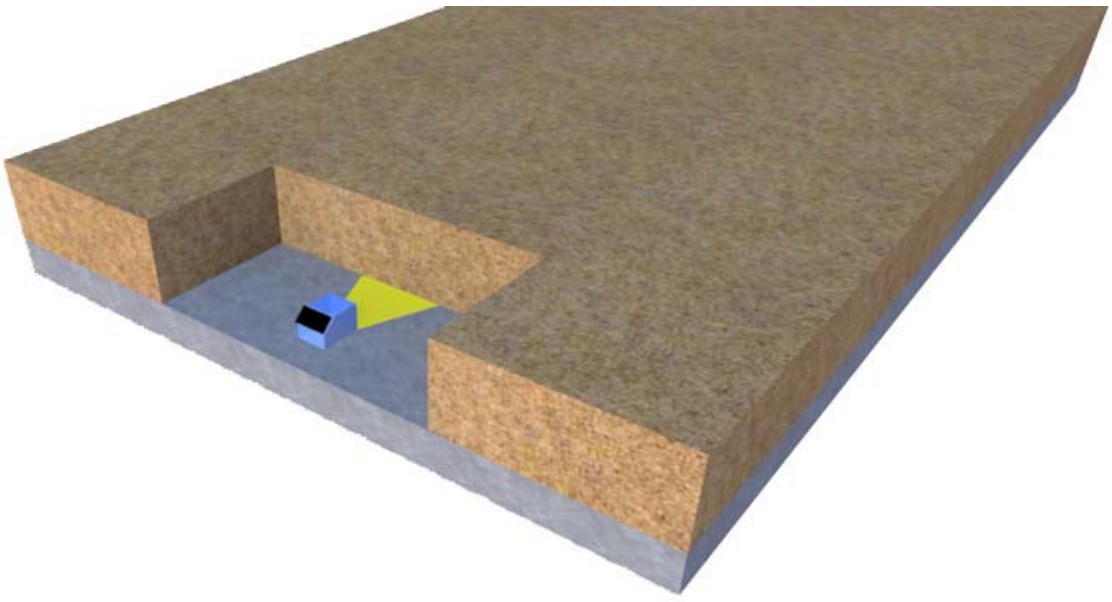

Figure 3.1: An inaccessible plate like a structure buried under soil. A section of the soil is dug away and ultrasonic guided waves are used to inspect the section under the soil. With correct mode and frequency selection, energy loss to the soil can be minimized.

In this work, a steel plate that is covered by a layer of wet saturated soil is considered as a prototype model. Figure 3.2 shows a photograph of this prototype. A 3/8 inch steel plate is covered by a thick layer of wet saturated soil. The length of the plate is 8 feet and width is 4 feet. The layered section is approximately 5 feet long and 1 foot wide. A 3/8 inches wide, 1 inch long and 100% through-wall anomaly at the end of the layered section is used as a benchmark for analysis in the sample experiments.

The aim of this work was to identify modes that have a minimum attenuation as they propagate along the waveguide formed by the buried steel plate in order to maximize the length of the structure that can be inspected from the end of the plate, or from any access point that can be created along its length.

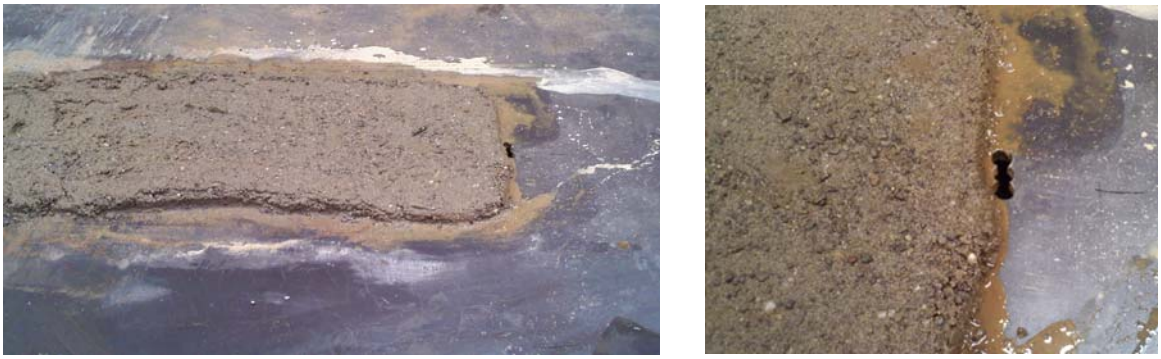

(a) (b)

Figure 3.2: (a) A 3/8” thick steel plate with a layer of wet saturated soil used as a working model. (b) A 3/8” wide, 1” long and 100% through-wall anomaly is used as a benchmark for sample experiments.

3.2 Excitation of Guided Waves

In principle, apart from laser generated ultrasound, two types of transducers, piezoelectric transducers and electromagnetic acoustic transducers (EMAT) are used in ultrasonic NDT. This chapter places emphasis on the excitation of Lamb type waves using piezoelectric transducers and the generation of SH-waves using EMATS. In the subsequent chapter, penetration power studies are carried for these two types of guided waves to determine the appropriate transducer for the given guided wave problem.

3.2.1 Lamb Wave Excitation

Strictly speaking, Lamb waves are waves of plain strain that occur in a traction free homogeneous and isotropic plate. Displacements occur both in the direction of wave propagation and perpendicular to the plane of the plate. An infinite number of modes can be generated in the plate due to this interaction. These modes propagate with different phase velocities and are generally dispersive (i.e. their velocities are frequency-dependent).

Dispersion causes the energy in the Lamb wave to spread out in both space and time as it propagates away from the source. [Cawley and Alleyne 1996] demonstrated an example where the signal-to-noise ratio reduces rapidly with distance along the plate for a dispersive wave mode; whereas it remains fairly constant for a non-dispersive wave mode. Thus, dispersion limits the propagation distance that can be achieved before the signal is lost into noise. Also, the increase in signal duration worsens the resolution that

can be obtained. The dispersion effect can be minimized by using an input signal with the narrowest bandwidth possible, which is one of the reasons why windowed tone bursts rather than pulses tend to be used as the input signals in Lamb wave applications.

In order to inspect large structures covering several feet, it becomes necessary to selectively excite and detect a single guided wave mode while suppressing coherent noise due to other modes of guided wave propagation. For this reason, the design of the transducer and the input signal are tailored such that the excitation energy is targeted at a single point on a suitable guided wave mode at a suitable frequency [Wilcox *et al* 2001]. Such points can be identified on a dispersion curve, a graph that shows all the constructive interference zones that occur as the ultrasonic waves reflect inside the structure. [Rose 1999] gives details for computing these phase and group velocity dispersion curves. Figure 3.3 is a plot of phase velocity dispersion curve for a steel plate of arbitrary thickness.

There are many different techniques for generating these Lamb type waves. [Rose 2002] demonstrated two techniques, one using an angle beam transducer and the other using a comb transducer. In this work, experiments have been conducted using a variable angle beam transducer.

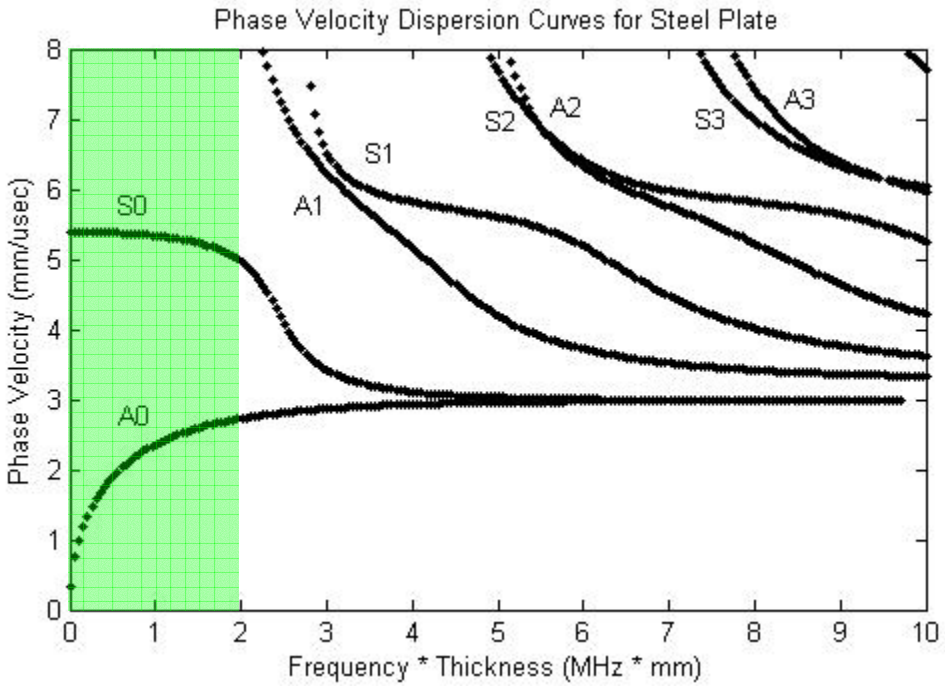

Figure 3.3: Phase velocity dispersion curves for a steel plate assuming a longitudinal bulk velocity of 5.85 mm/µsec and a shear bulk velocity of 3.23 mm/µsec. The shaded green zone shows the frequencies below the cut-off frequencies of all higher order modes.

In an angle incidence configuration, a conventional bulk wave transducer is positioned at an angle above the surface of the plate under inspection as shown in Figure 3.4 (a). The transfer of energy from an ultrasonic probe into a specimen via an air gap is virtually impossible and for this reason some form of coupling material has to be provided [Silk 1984]. When used to transmit, the transducer excites plane bulk compression waves in the coupling medium that impinge on the surface of the plate at an angle. This causes a spatially and temporally periodic distribution of out-of-plane surface stresses or tractions to be set up on the surface of the plate. The spatial periodicity of the surface tractions causes the angle incidence technique to preferentially excite Lamb waves with a certain phase velocity. Based on the angle at which the transducer is positioned, different Lamb wave modes can be generated.

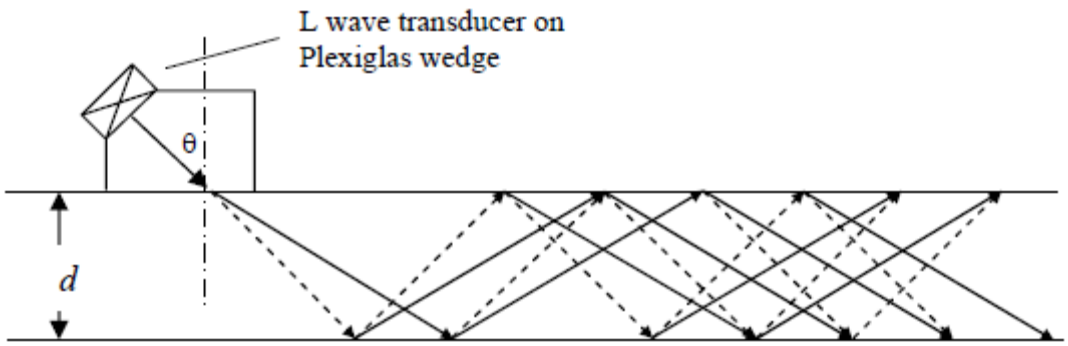

(a) Angle Wedge Transducer

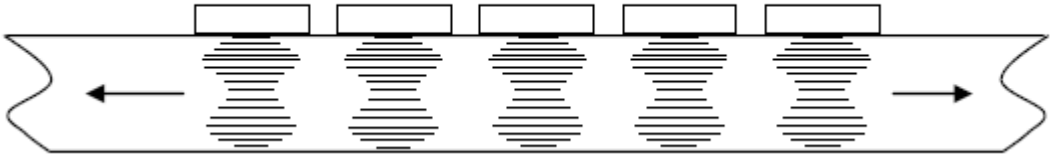

(b) Comb Transducer

Figure 3.4: 'Lamb type' wave generation in a plate. [Rose 2002]

Each wave mode excited in the plate will have its own profile of in-plane and out-of-plane energy distribution throughout the structure. This representation is depicted in the form of wave structure plots as shown in Figure 3.5 (a) and (b) for two frequencies. Wave structure generally changes as we move along a mode in the phase velocity dispersion curves and has an important role to play in mode selection for inspection of different structures.

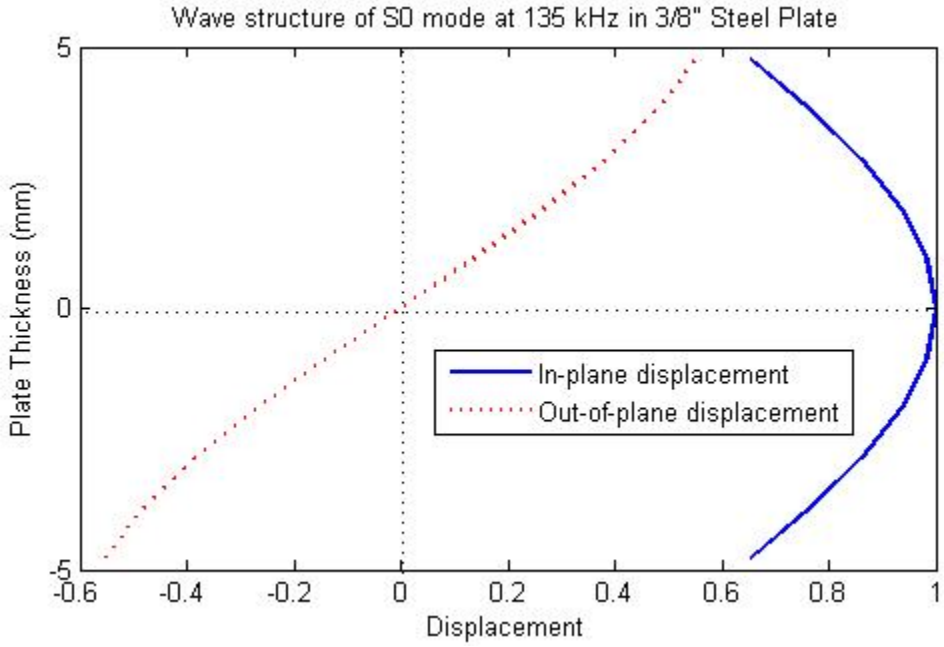

(a)

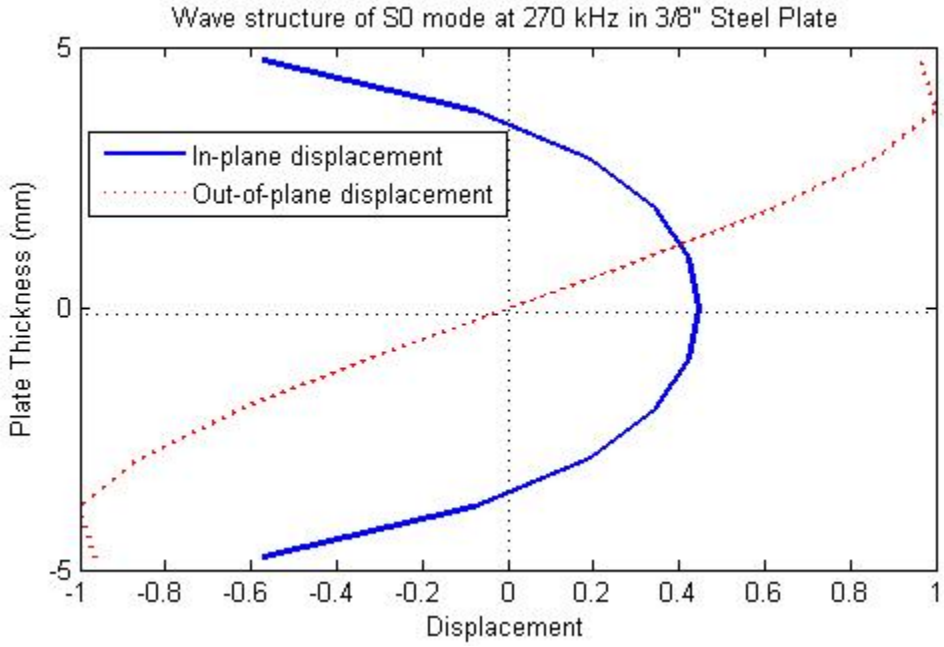

(b)

Figure 3.5: Wave structure for the S0 mode at (a) 135 kHz and (b) 270 kHz in a 3/8" plate. Observe that in (a) there is complete in-plane dominance throughout the plate thickness whereas in (b) out-of-plane is dominant at upper and lower surfaces of plate.

.

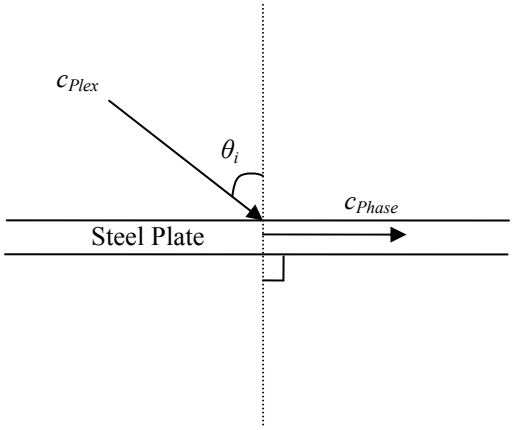

Figure 3.6: Snell's Law for angle determination to excite a single guided wave mode. c_{Plex} is the phase velocity of the excited mode in Plexiglas and c_{Phase} is obtained from the phase velocity dispersion curve for a steel plate, Figure 3.3**.**

Following the notation of [Rose 1999], in order to excite a single guided wave mode, Snell's law can be used to determine the wedge angle as shown in Figure 3.6. The relation between the longitudinal wave velocity in Plexiglas (c_{Plex}) and that in the steel plate (c_{Phase}) is described by Equation 3.1.

$$\frac{\sin\theta_i}{c_{Plex}} = \frac{\sin 90^\circ}{c_{Phase}} \qquad [3.1]$$

The shaded green zone shown in Figure 3.3 covers all those frequencies below the cutoff frequencies of the higher order modes. As can be seen, only the fundamental symmetric and anti-symmetric modes can be generated in this zone. An advantage of exciting a mode in this zone is that there are lesser chances of mode conversions. For the given problem, a non-dispersive mode having dominant in-plane displacement would serve the purpose. Based on all these factors, the S0 mode at 190 kHz was identified to look for anomalies under the buried plate.

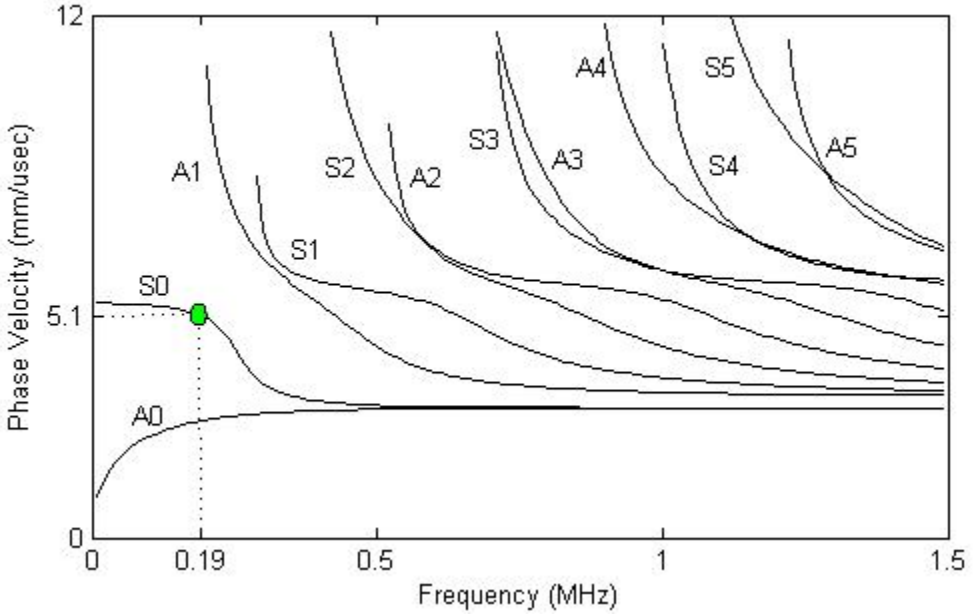

Figure 3.7: Lamb waves phase velocity dispersion curves for a 3/8 inch thick steel plate assuming a longitudinal bulk velocity of 5.85 mm/µsec and a shear bulk velocity of 3.23 mm/µsec. The S0 mode is shown to be excited at 190 kHz.

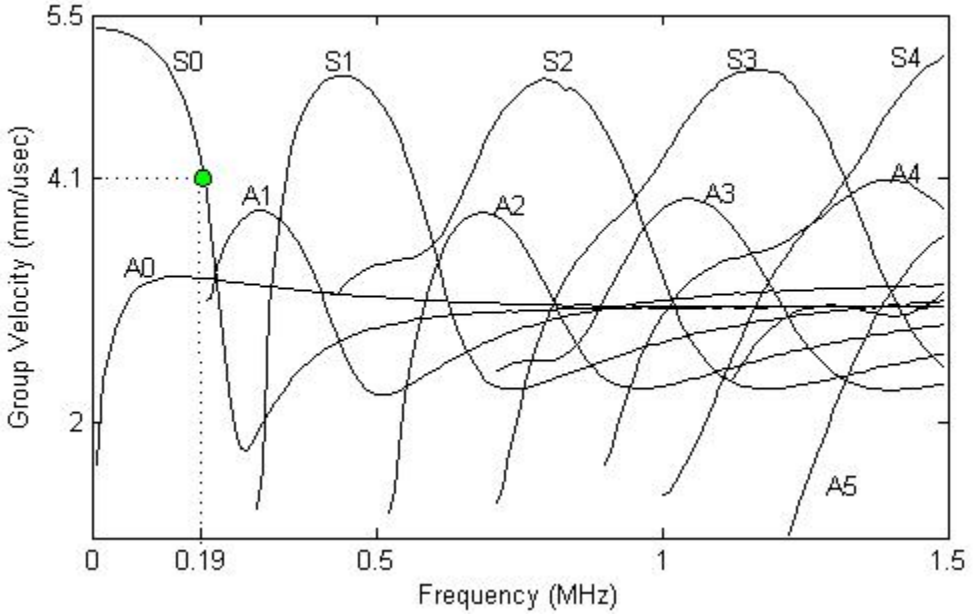

Figure 3.8: Lamb waves group velocity dispersion curves for the steel plate of Figure 3.7. The group velocity of the excited S0 mode is shown to be 4.1 mm/µsec.

The dispersion curve shown in Figure 3.3 has a frequency-thickness product on its horizontal axis. Since all experiments included in this chapter are carried out on a steel plate of known thickness (3/8 inch), it is more convenient to use a phase velocity dispersion curve with only frequency on the horizontal axis. In Figure 3.7, the S0 mode is shown to be excited at a frequency of 190 kHz. The phase velocity is valued at 5.1 mm/μsec. Figure 3.8 shows the group velocity dispersion curve for the 3/8 inch thick steel plate.

3.2.2 Shear Horizontal Wave Excitation

Apart from the Lamb wave modes that exist in flat layers, there also exists a set of time harmonic wave motions known as shear horizontal (SH) modes. In these modes, the particle vibrations are entirely in-plane, orthogonal to the direction of wave propagation. So, a forward propagating wave has side-to-side oscillatory particle motion.

EMATs are an efficient method used to generate SH waves. An SH wave EMAT generally consists of a race-track shaped current carrying coil as shown in Figure 3.9 and a cluster of permanent periodic magnets. It works under the Lorentz force principle in a non-ferromagnetic metal. The oscillating current in the face coil induces oscillatory eddy current at the surface of a metal close to the face coil. Under the magnetic field of the permanent magnets or electromagnets, the induced eddy current will exert vibration force to the lattice of metal microstructure, which in turn induces mechanical vibration in the material. For a detailed analysis on the intricacies of the SH wave EMAT, one is pointed

to [Vasile and Thompson 1977]. More recent EMAT applications can be found in [Hirao and Ogi 2003].

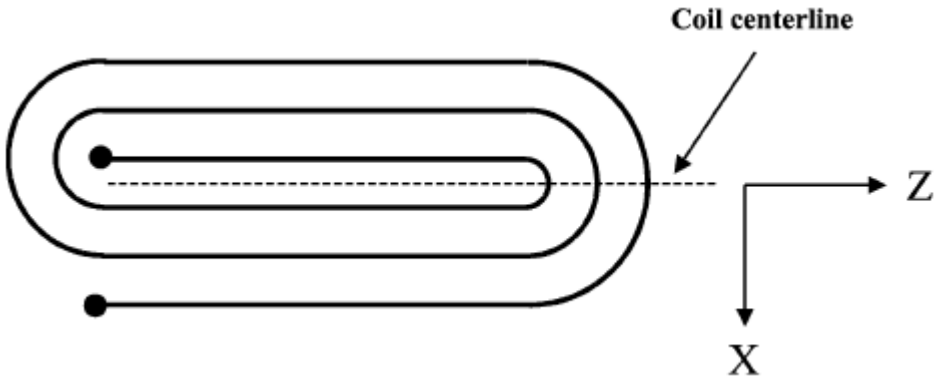

Figure 3.9: A race-track shaped current carrying coil used to generate SH-waves. [Mirkhani *et al* 2004]

In order to obtain the SH dispersion curves for the steel plate, the material constants must be known. Bulk longitudinal wave and shear wave measurements were taken at various positions on the plate. Guided wave group velocity measurements were also taken at various angles throughout the plate. Isotropy was assumed because variation in group velocity was small enough to be negligible in different propagation directions. From the elastic constants obtained, phase and group velocity dispersion curves were generated for the SH waves for a 3/8 inch thick steel plate as shown in Figure 3.10 [Rose 1999].

The spacing length of the alternating magnets in the wave propagation direction determines the slope of the excitation line that runs from the origin across the dispersion curve (dashed line in Figure 3.10). Equation 3.2 shows this relation.

$$\lambda = 2d = \frac{c_p}{f} \qquad [3.2]$$

Here, λ is the wavelength of the SH wave to be generated, d is the distance between the center of the two adjacent alternating magnets, c_p is the phase velocity, and f is the excitation frequency.

Thus, the slope of the excitation line is just the wavelength of the SH wave. When this excitation line crosses a particular mode on the dispersion curve, that mode will be excited at the given excitation frequency also called as a peak frequency [Luo and Rose 2003]. Figure 3.11 illustrates the group velocity curves for the SH wave family.

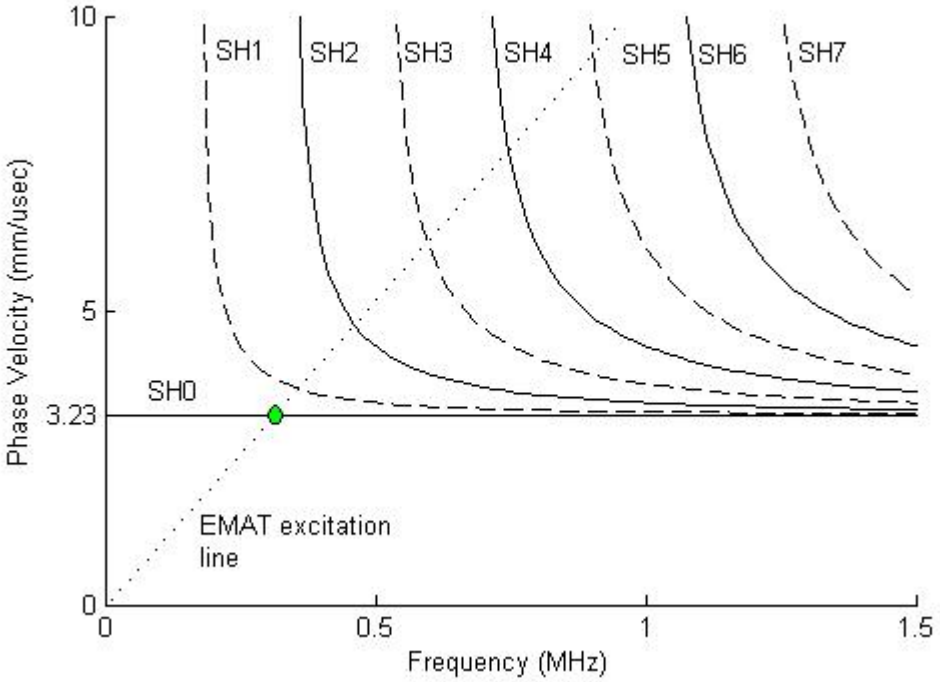

Figure 3.10: SH waves phase velocity dispersion curves for a 3/8 inch thick steel plate assuming a shear bulk velocity of 3.23 mm/μsec. Solid curves denote symmetric modes; dashed curves denote antisymmetric modes.

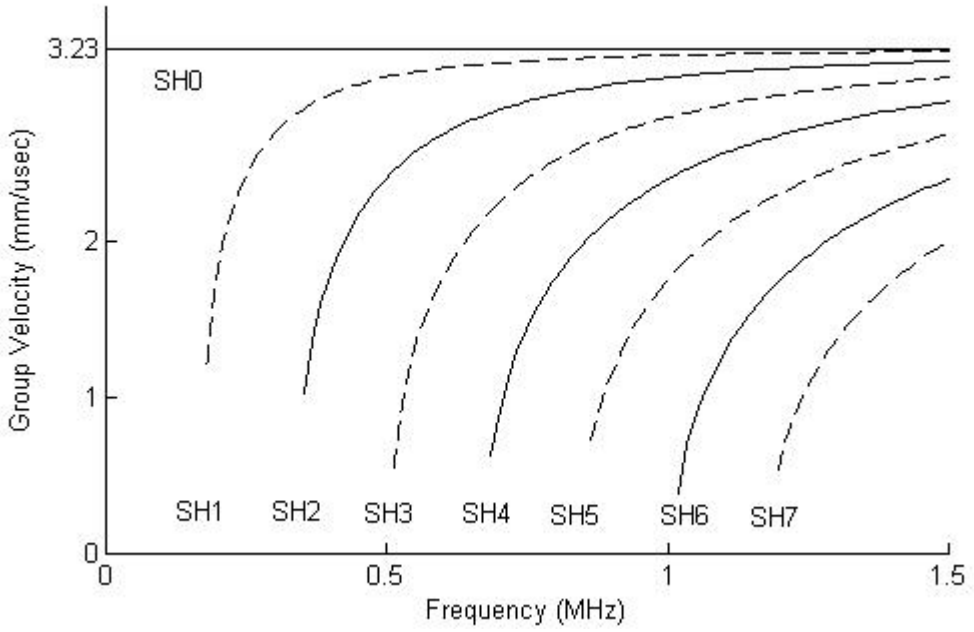

Figure 3.11: SH waves group velocity dispersion curves for the steel plate of Figure 3.9. The fundamental SH0 mode is non-dispersive and has a group velocity of 3.23 mm/μsec.

The fundamental SH mode is the SH0 (symmetric) mode. The properties of this mode are frequency independent: it is completely non-dispersive at all frequencies and its phase velocity is the bulk shear velocity. The next mode appearing is the SH1 (anti-symmetric) mode and so on. [Fortunko *et al* 1982] showed the use of the SH0 and SH1 plate modes for detecting and sizing crack-like defects in plates. Due to its non-dispersive property, the SH0 mode was identified as the preferred mode for further experiments.

3.3 The Guided Wave Inspection Method

In order to know what type of guided wave needs to be used, it is prudent to look at an example of a civil structure where the inspection system can be fully utilized. Figure

3.12 looks at a plate-like structure buried under soil with concrete reinforcements at the bottom of the plate. This could well be a cross-section of an underground roadway.

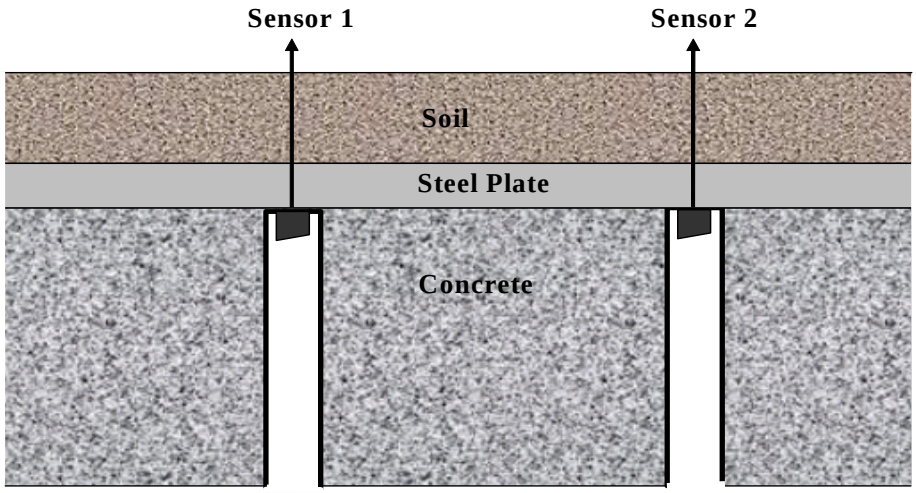

Figure 3.12: Cross-section of a potential plate-like structure that could be inspected with the guided wave inspection system being developed. Holes are drilled through the concrete to gain access to some part of the plate in order to inspect it.

As depicted in the figure, two sensors are mounted on the plate to inspect it. Figure 3.13 illustrates a method of 'random sampling' of the entire structure to inspect different areas.

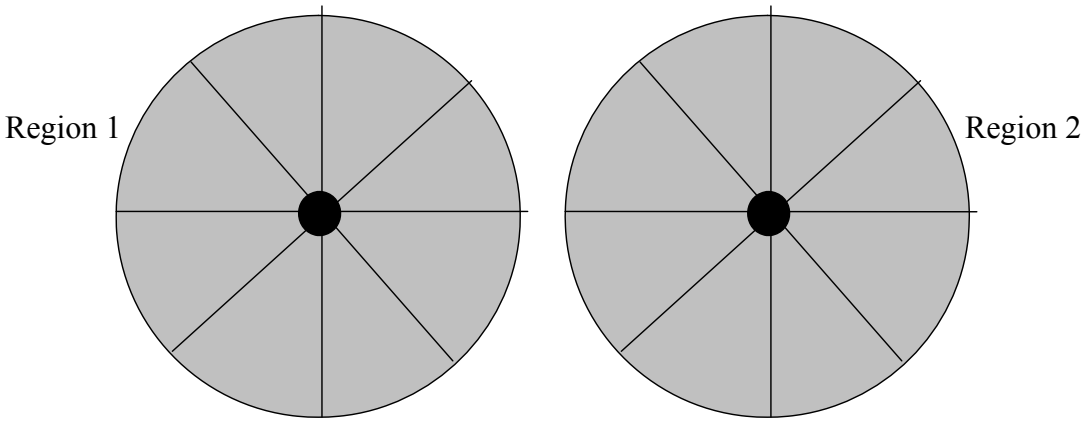

Figure 3.13: Top view of the scenario shown in Figure 3.12. The sensors are at the center of the two regions. A complete 360˚ scan of each region can be done by each sensor by a simple rotation. The two sensors can also operate in a through transmission mode and look at anomalies between them.

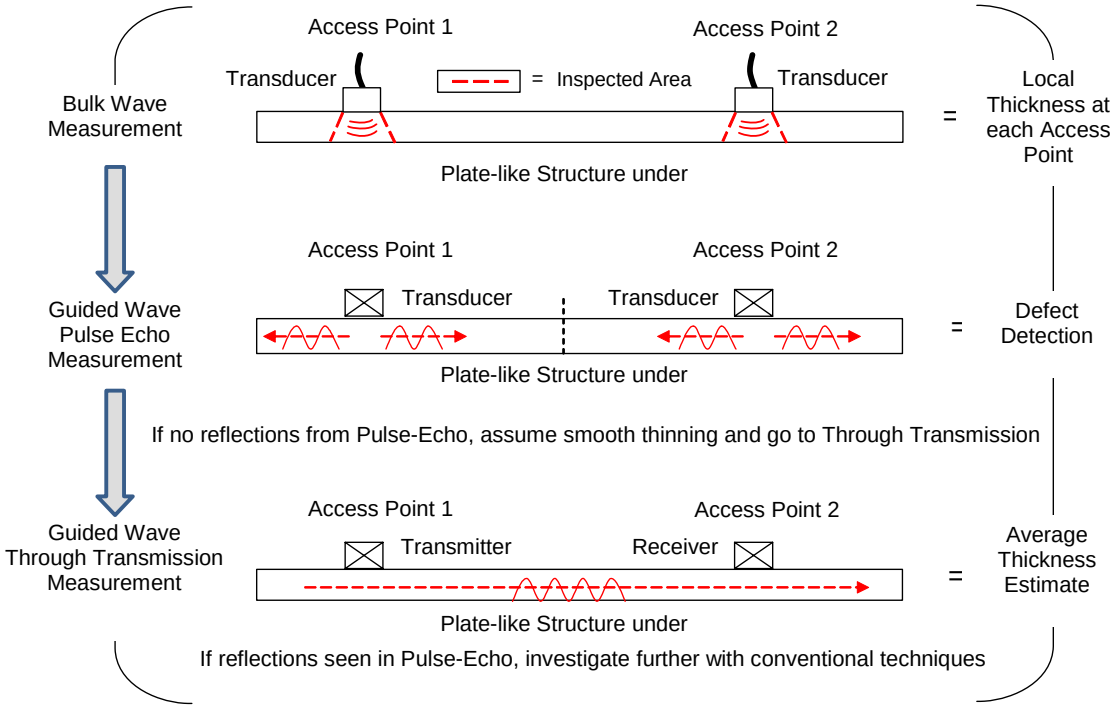

Figure 3.14: A three stage inspection methodology.

Based on Figure 3.12 and Figure 3.13, an inspection methodology is proposed as shown in Figure 3.14. The first stage is a local bulk wave measurement which provides information only about that access point. Next is a guided wave pulse echo measurement. In this stage, at each access point a pulse-echo signal is sent in all directions to inspect for sharp discontinuities. In case defect reflections are observed in these signals, further investigation should be done in that region or zone. Finally, a transmitter and receiver are operated in a through transmission mode to look for gradual thinning-like changes, thus completing the inspection procedure.

CHAPTER 4

PENETRATION POWER STUDIES

In order to determine the guided wave that will best solve the problem at hand, penetration power studies were carried out for both Lamb and SH waves. For this an amplitude decay study was performed over a 5 feet range using the through-wall defect as a reference.

4.1 Lamb Wave – The S0 Mode

Based on the facts highlighted in the previous chapter, the S0 mode at 190 kHz was used for this study. Figure 4.1 shows a photograph of the experimental setup. A 500 kHz variable angle wedge transducer, having angle set at 31˚ based on Snell's law, was setup on the steel plate at a distance of 2 feet from the anomaly. The signal obtained (black line) is shown in Figure 4.2. A layer of wet sand approximately 2 feet long, 1 foot wide and 1 inch thick was then placed between the transducer and the anomaly. In this case, the signal level of the anomaly reflection (blue line) dropped to almost half of its original value. Table 4.1 summarizes the results concluded from Figure 4.2.

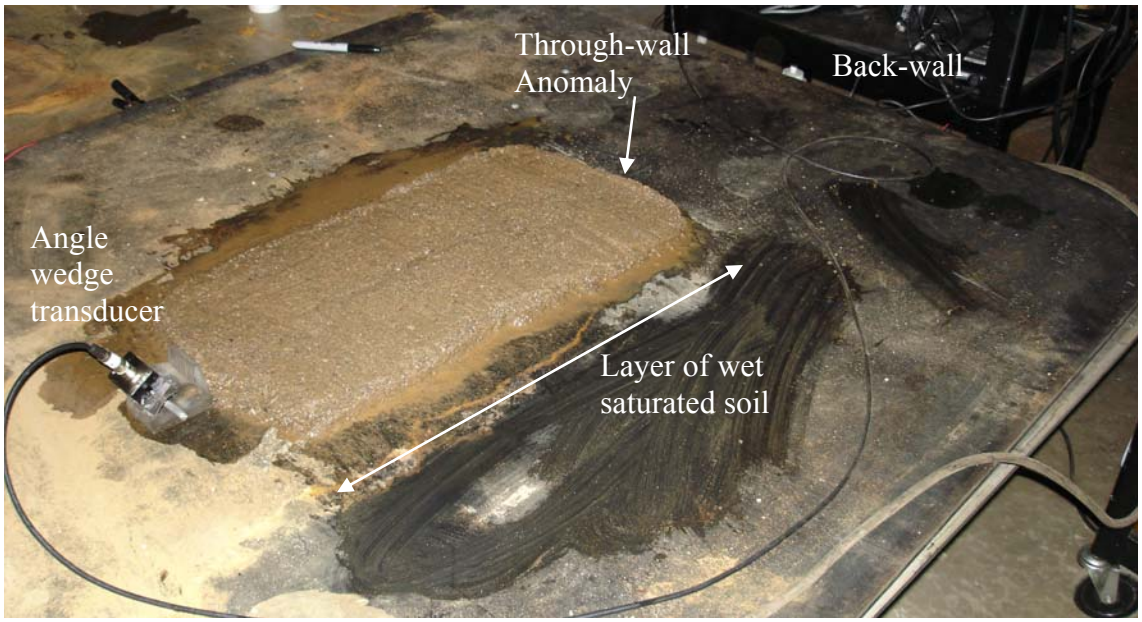

Figure 4.1: Photograph showing a variable angle wedge transducer setup to send the S0 wave mode at 190 kHz underneath a 2 feet long layer of saturated soil.

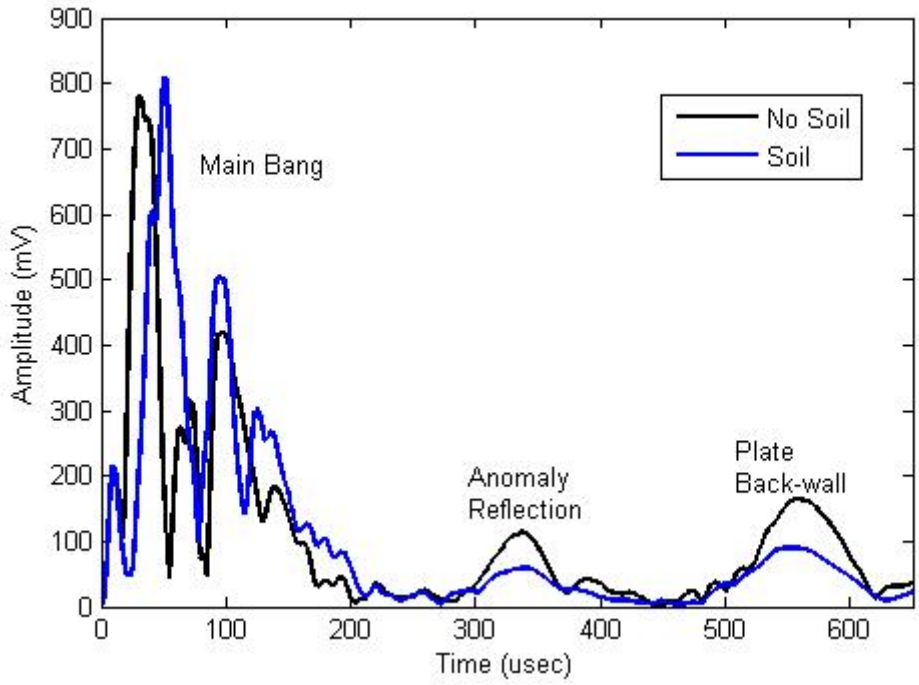

Figure 4.2: Analytic envelopes of RF waveforms obtained from S0 wave propagation with no soil (black line) and with 2 feet of saturated soil (blue line). The S0 mode was used here at a frequency of 190 kHz.

Table 4.1: Defect location based on a group velocity of 4.1 mm/µsec for the S0 mode at 190 kHz.

	Travel Distance (mm)	Theoretical Defect Location (µs)	Experimental Defect Location (µs)	Amplitude (mV)	Attenuation (dB)
No Soil	1295.4	315.95	337	113.6	-
Soil	1295.4	315.95	335	58.29	5.795

The transducer was then moved to a distance of 3 feet from the anomaly and more wet sand was placed in between. Another reading was taken. Similarly, another reading was taken at a distance of 4 feet from the anomaly. Figure 4.3 illustrates the results of this study.

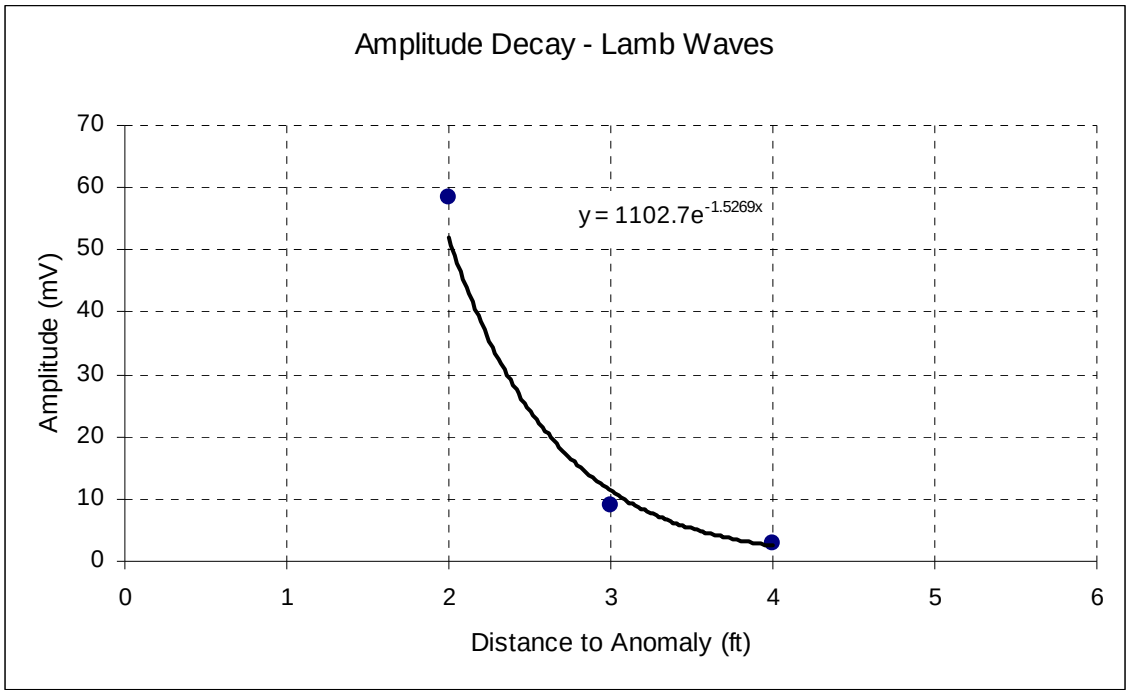

Figure 4.3: Exponential decay in anomaly reflection amplitude as the angle wedge transducer is moved progressively farther away from the anomaly. Blue dots denote data points. The black line represents an exponential fit to these data points.

4.2 SH Wave Studies – The SH0 Mode

The fundamental non-dispersive mode of the SH guided wave family was used for this study. Figure 4.4 shows a photograph of the experimental setup. The EMAT was placed with receiver first at a distance of 2 feet from the defect. The transmitter was 3 inches further away from the defect as shown in the photograph below. Thus the total travel distance for the SH0 mode was 51 inches or 1295.4 mm.

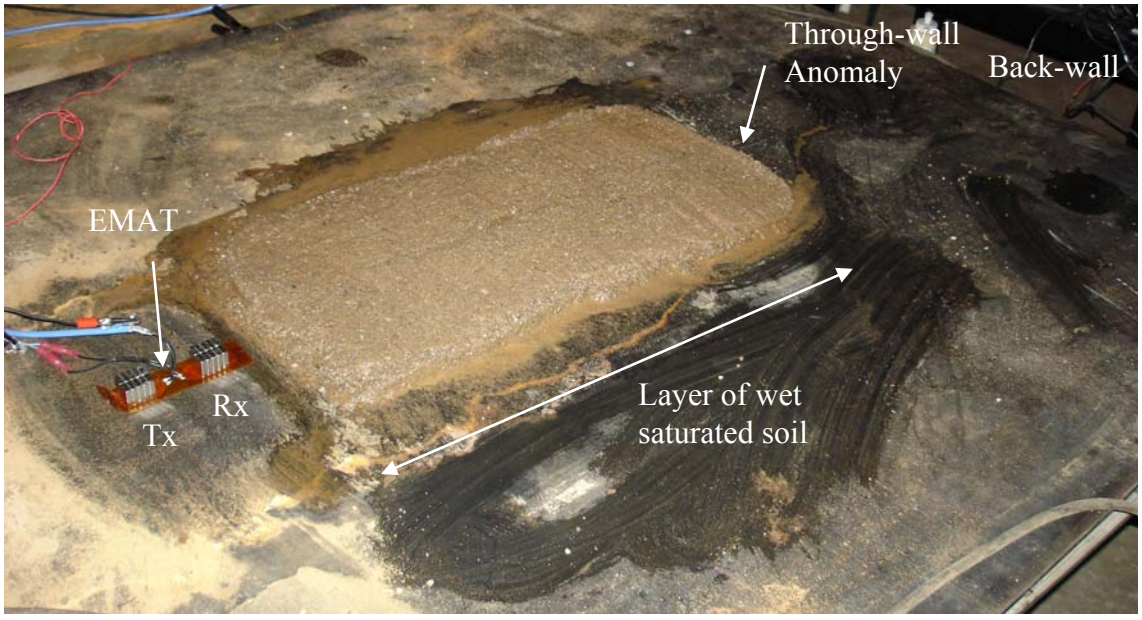

Figure 4.4: Photograph showing an Electromagnetic Acoustic Transducer (EMAT) arranged to send the SH0 wave mode at 275 kHz underneath a 2 feet long layer of wet saturated soil.

Based on the dispersion curves shown in earlier, the SH0 mode should be generated at an operating frequency close to 300 kHz. By tuning frequencies in the range of 250 - 300 kHz, it was found that the SH0 mode was aptly being generated at a frequency of 275 kHz. Figure 4.5 shows the results for the detection of the through-wall

anomaly from a distance of 2 feet without wet sand (black line) and with wet sand (red line). Table 4.2 summarizes the results concluded from Figure 4.5.

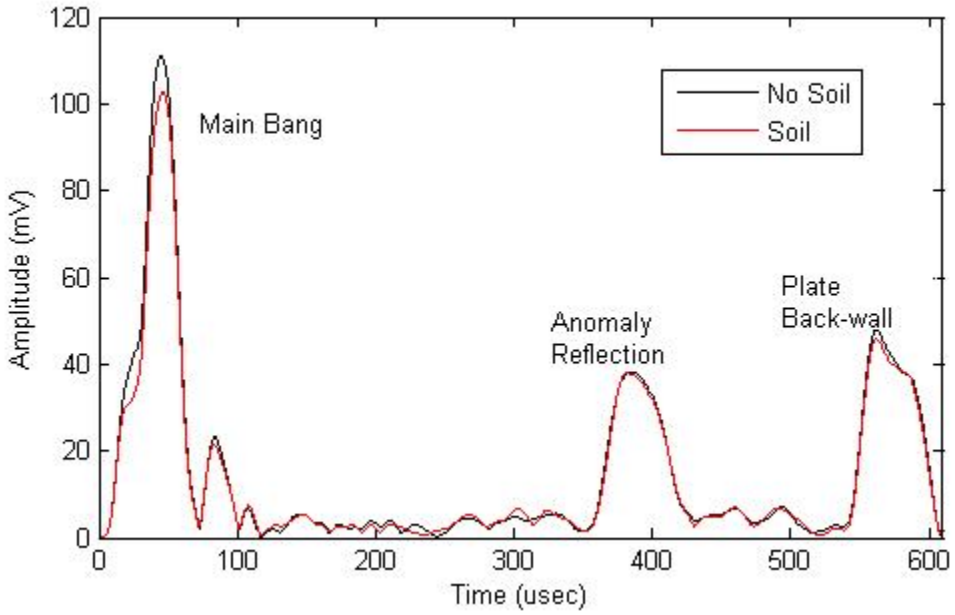

Figure 4.5: Analytic envelopes of RF waveforms obtained from SH0 wave propagation with no soil (black line) and with 2 feet of saturated soil (red line). The SH0 mode was used here at a frequency of 275 kHz.

Table 4.2: Defect location based on a group velocity of 3.23 mm/µsec for the SH0 mode at 275 kHz.

	Travel Distance (mm)	**Theoretical Defect Location (µs)**	**Experimental Defect Location (µs)**	**Amplitude (mV)**	**Attenuation (dB)**
No Soil	1295.4	401	385.3	38.12	-
Soil	1295.4	401	384	37.85	0.06

Figure 4.6 shows the results from a similar amplitude decay study in which the transducer was moved progressively farther away from the anomaly in 1 foot increments. The echo amplitude values corresponding to the anomaly are plotted and an exponential

fit to these results is shown which allows for the estimation of total potential inspection distance from a single location.

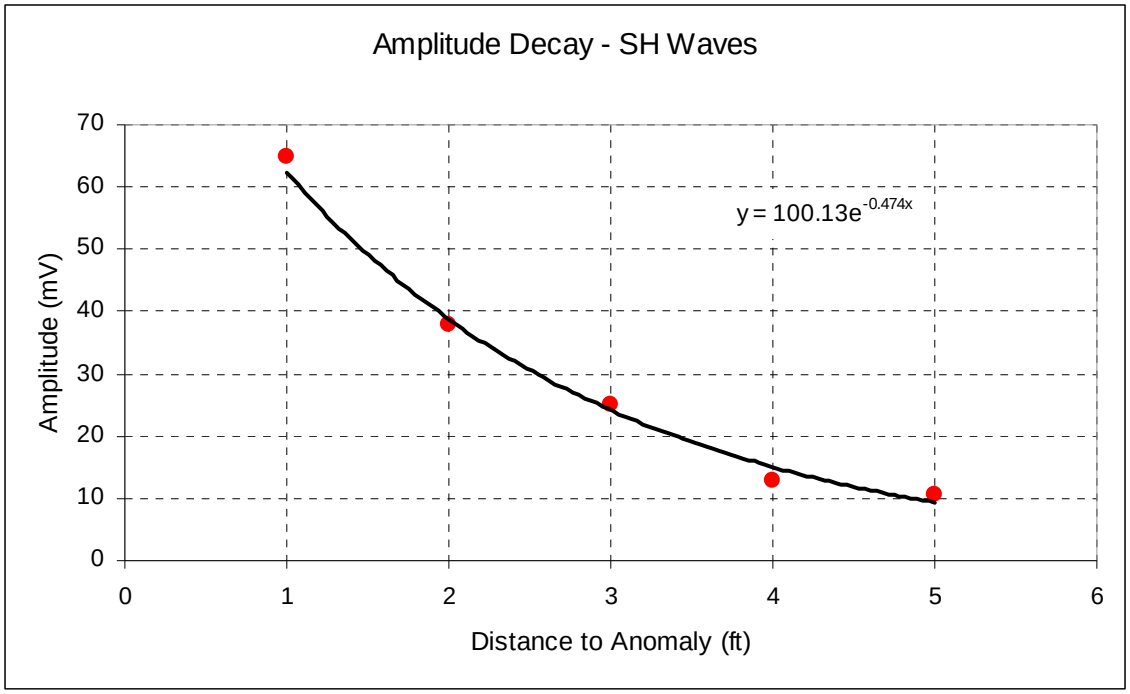

Figure 4.6: Exponential decay in anomaly reflection amplitude as the EMAT is moved progressively farther away from the anomaly. Red dots denote data points. The black line represents an exponential fit to these data points.

4.3 Discussion on Penetration Power Study

Reviewing Figure 4.3, Figure 4.6, Table 4.1 and Table 4.2, the following observations can be made:

- Attenuation caused by wet sand is more severe for the S0 mode than for the SH0 mode.

- The amplitude decay curve is steeper for the S0 mode than for the SH0 mode.

- Assuming a noise floor of around 5 mV, which is typical of the collected signals, the total potential inspection distance from a single location, is around 6.32 feet in a single direction when using the SH0 mode. On the other hand, the amplitude level for the S0 mode drops below the assumed noise floor at a distance of 4 feet from the anomaly, thus limiting its maximum distance inspection capability.

- Operating in a through-transmission mode, the EMAT was able to separate the anomaly reflection from the main bang even from a distance of 1 foot. In the case of the 500 kHz wedge angle transducer operating in a pulse echo mode from 1 foot, the anomaly reflection was lost in the main bang, thus hindering its minimum distance inspection capability.

Based on these observations, it can be concluded that the SH0 mode shows more promise in identifying anomalies in plate or plate-like structures that are buried under wet sand.

CHAPTER 5

BEAM PROFILE OF SH WAVE EMAT AND PLANAR DEFECT ANALYSIS

It is important to know the beam width of an EMAT at its operating frequency. Beam spreading may result in the detection of an anomaly that is off the centerline of the sensor, which is not necessarily bad. Based on beam directivity, the sensitivity of the EMAT towards cracks is also studied in a later section of this chapter.

5.1 Beam Width Determination

In order to determine the beam spread, the EMATs were used in a through-transmission mode, where the transmitter-receiver pair was kept at:

i) 2 feet away from each other

ii) 3 feet away from each other

The transmitter EMAT is bidirectional and hence two SH-wave signals are generated that travel in opposite directions normal to the coil; one towards the receiver EMAT and the other away from it. Figure 5.1 shows the technique adopted to determine the beam spread of the EMAT sensor.

In this experiment, the transmitter position was fixed and the receiver was *rastered* along the width of an 8 foot by 4 foot steel plate in a direction perpendicular to the transmitter. The plate was 3/8 inch thick. Fifteen readings, at intervals of 3 inches each, were taken using the SH0 mode at 275 kHz for each of the above two runs of the experiment. The amplitude of the received signal was then plotted for each of these fifteen points and the beam spread spectrum was calculated and is shown in Figure 5.2.

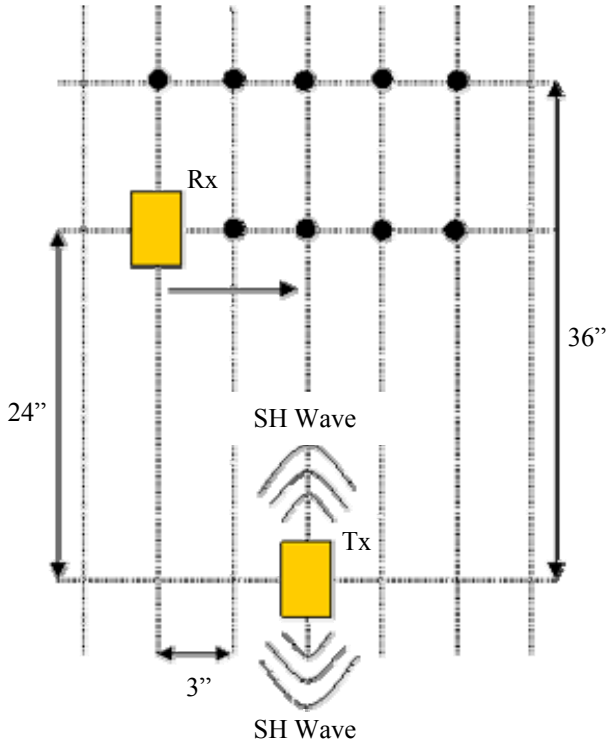

Figure 5.1: Experiment to determine the beam profile and beam width of EMAT transmitter. The transmitter coil was kept fixed while the receiver coil was moved along the raster grid represented by the black dots. Operating frequency of the transmitter was 275 kHz generating the SH0 mode. (Diagram is not to scale).

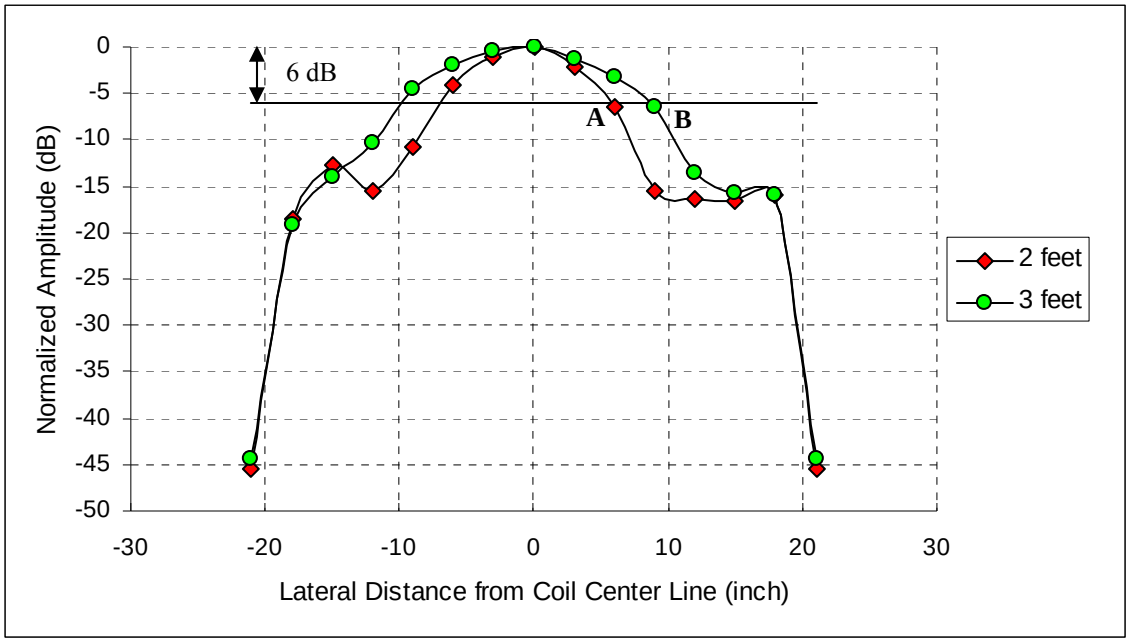

Figure 5.2: Beam divergence plot of EMAT generating the SH0 wave at an operating frequency of 275 kHz. Red diamonds represent data points taken by the receiver coil at a distance of 2 feet from transmitter coil. Green dots represent data points taken by the receiver coil at a distance of 3 feet from receiver coil. Data points A and B are the 6 dB cut-off points for distances corresponding to 2 feet and 3 feet respectively.

Figure 5.3 shows the geometrical representation of the experiment that was performed to determine the beam width of the EMAT sensor. The red and green lines in the figure correspond to the loci of all scan points at an axial distance of 2 feet and 3 feet respectively from the transmitter. Points A and B correspond to the horizontal offset of the receiver coil at which point the signal amplitude has dropped by 6 dB.

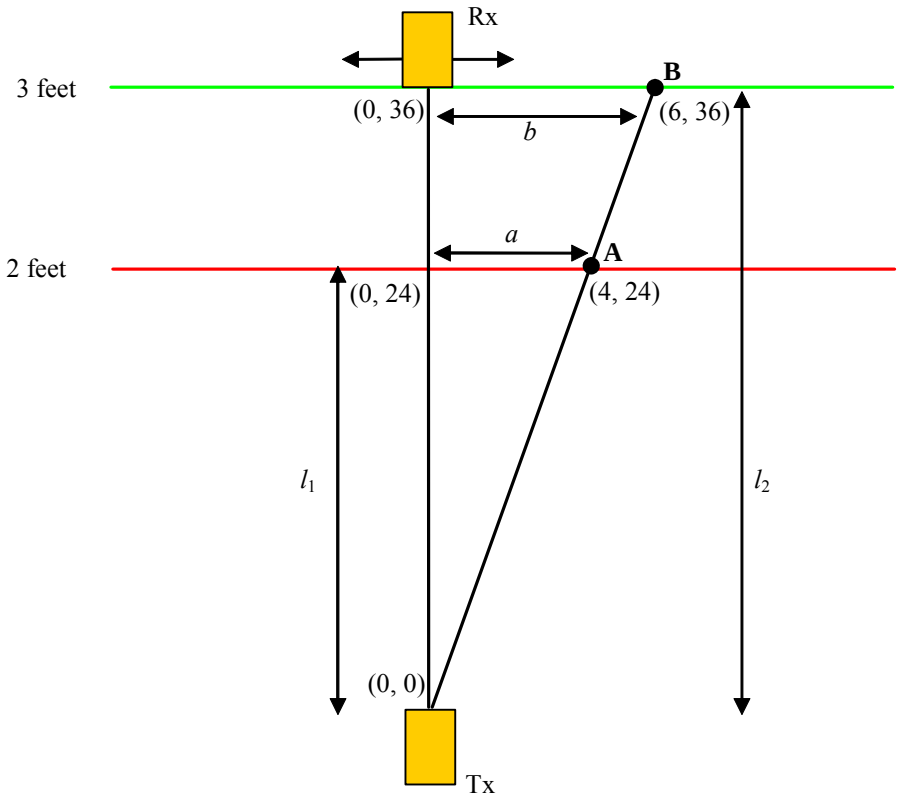

Figure 5.3: Geometrical representation of experimental setup used to determine the amount of beam spreading that occurs from the EMAT transmitter using the SH0 mode at 275 kHz. Points A and B in the illustration correspond to the horizontal offset of the receiver coil at which point the signal amplitude has dropped by 6dB.

For the first run of the experiment the distance between transmitter and receiver was 2 feet (24 inches). Using a 6 db drop from the peak amplitude as a reference, the angle of divergence, $\theta_{2\,ft}$ for the EMAT was then calculated as per Equation 5.1.

$$\theta_{2\,ft} = \arctan\left(\frac{a}{l_1}\right) = 9.46^{\circ} \qquad [5.1]$$

For the second run of the experiment, where the distance between transmitter and receiver is 3 feet (36 inches), the angle of divergence, θ_{3ft} is calculated as per Equation 5.2.

$$\theta_{3ft} = \arctan\left(\frac{b}{l_2}\right) = 9.46^{\circ} \qquad [5.2]$$

Based on these two runs, it can be concluded that the angle of divergence for the EMAT is 9.46˚ for the SH0 mode at a frequency of 275 kHz. Therefore, an anomaly located at an axial distance of 10 feet may potentially be detected as far as 20 inches off the centerline. This is acceptable, giving a better chance of detection as corrosion can change slope and different impingement angles might be better. The locus of points that could contain the defect would at least be known. Figure 5.4 shows a top view of the beam profile of the EMAT.

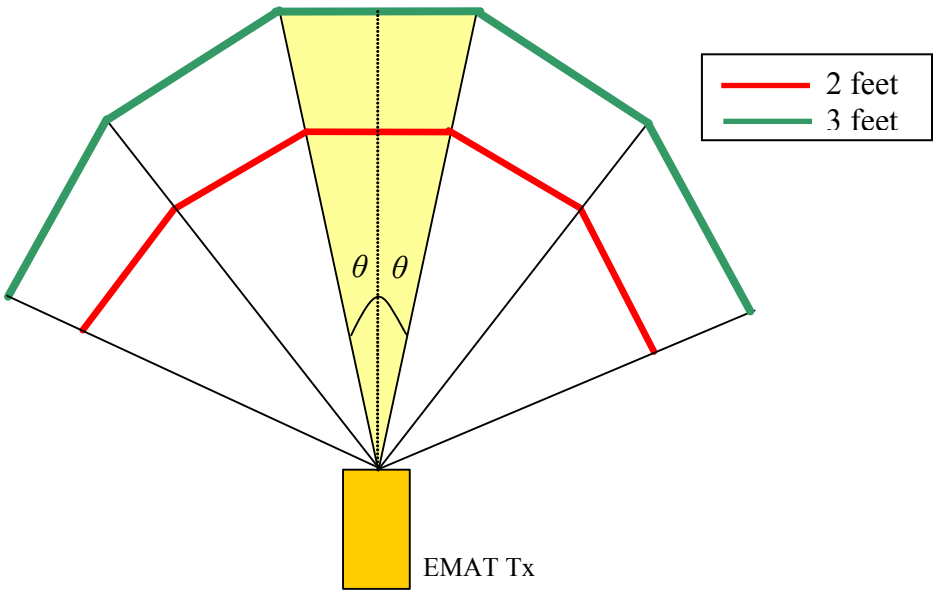

Figure 5.4: Beam profile of the EMAT transmitter where θ is the beam width. If d is the maximum range of the EMAT then the total inspected region covered by the EMAT can be approximated to be a triangle having an area of $d^2 \tan(\theta)$ as shown in pale yellow.

5.2 Planar Defect Study

[Fortunko *et al* 1982] showed the usefulness of SH waves for the detection and sizing of planar defects like cracks in an isotropic metal plate. Based on the beam width determination in the previous section, a sensitivity analysis was performed to understand the given EMAT's capability to detect cracks using the SH0 mode.

A 50% through-wall, 6 inch wide crack-like defect was fabricated on the 3/8 inch thick steel plate as shown in Figure 5.5 (a). The EMAT sensors were setup in a pitch-catch arrangement at an axial distance of 2 feet from this defect and three different lateral positions relative to the center of the crack. Figure 5.5 (b) shows one such setup where the EMAT sensor pair was at a lateral offset of 3 inch from the center of the crack. Figure 5.6 illustrates the waveforms for all three positions.

(a) (b)

Figure 5.5: (a) A 50% through-wall, 6 inch wide crack-like defect. (b) EMAT sensors setup in pitch-catch arrangement at an axial distance of 2 feet and a lateral offset of 3 inch from the defect.

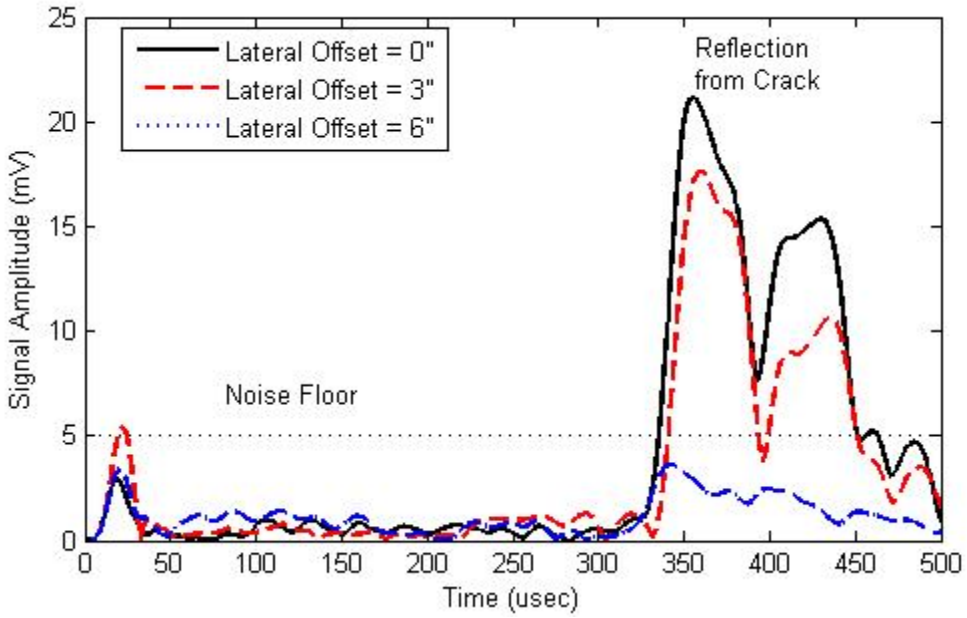

Figure 5.6: Analytic envelope of the signals obtained at three different lateral offsets from center of crack-like defect. The EMAT sensors were setup in a pitch-catch arrangement at an axial distance of 2 feet from the defect.

Figure 5.6 clearly ratifies the results of the previous section. From an axial distance of 2 feet and a horizontal offset of 3 inches from the center of the crack, a good reflection was obtained (red dashed line). However, when the sensor pair was moved to a horizontal offset position of 6 inch, the reflection echo (blue dashed line) fell below the noise floor of 5 mV thus giving a sensor beam width of around 9°.

5.2.1 Penetration Power Study

A penetration power study was carried out on the crack-like defect to interrogate the maximum distance from where the EMAT sensor could locate it. The procedure followed for this study was similar to one carried out earlier. Figure 5.7 shows the results of this study.

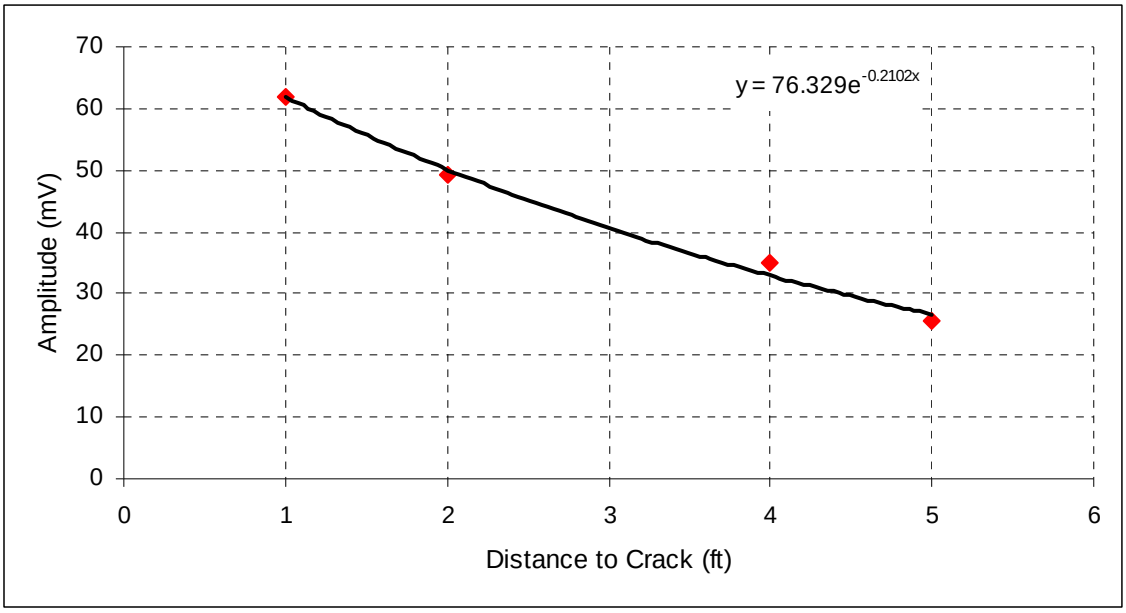

Figure 5.7: Exponential decay in crack-like defect reflection amplitude as the EMAT is moved progressively farther away from the anomaly. Red diamonds denote data points. The black line represents an exponential fit to these data points.

5.3 A Brief Experiment with Concrete

Another experiment was setup to analyze SH-waves propagating in a plate buried under concrete. Figure 5.8 (a) shows the 8 foot by 4 foot steel plate having the fabricated crack at the far end. The EMAT sensors were setup as shown in a pitch-catch arrangement and one signal locating the crack was captured. Then, concrete was poured in and leveled out as shown in Figure 5.8 (b) after which a signal waveform was taken every hour as the concrete dried up. Figure 5.9 shows the analytic waveforms of the SH wave signals captured for Figure 5.8 (a) and (b) in black and blue respectively. It can be seen that the wet concrete has very little effect on the amplitude of the reflection from the crack. However what is more interesting to note is the amplitude of echo reflection as the

concrete cured. Signals were taken every hour for the first four hours as the concrete stiffened. Another signal was obtained 24 hours later when the concrete had completely dried up. Figure 5.10 shows the trend of the amplitude levels.

(a) (b)

Figure 5.8: Experimental setup to test effect of concrete on SH-waves in a steel plate. (a) Signal taken before concrete was poured into the wooden frame. (b) Concrete was poured into the wooden frame and signals were taken every hour for four hours as the concrete set.

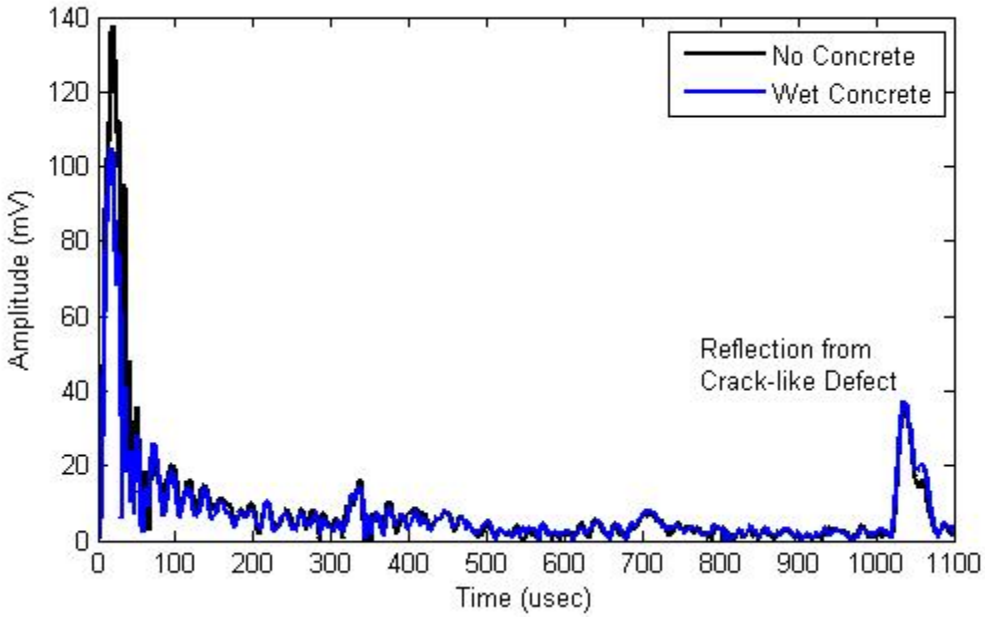

Figure 5.9: Analytic waveforms of the signals captured with no concrete (black line) and with wet concrete (blue line). The reflection from the crack is clearly seen from a distance of 5.5 feet from it.

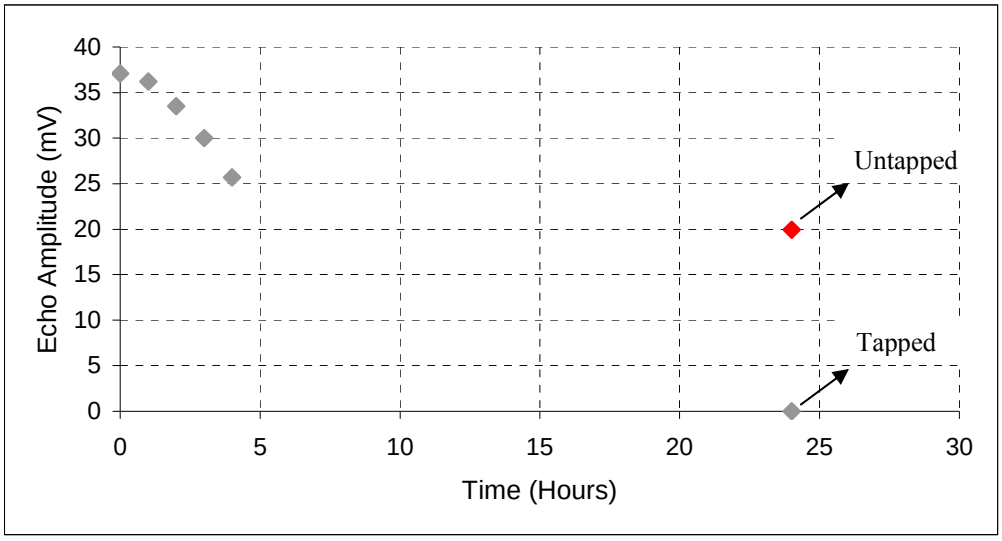

Figure 5.10: Echo reflection amplitude values (grey diamonds) were recorded every hour for the first four hours as the concrete stiffened. Another reading was taken 24 hours later for dry concrete.

5.4 Summary of Experimental Results

Based on the experiments conducted on beam width determination of the SH-wave EMAT and its sensitivity to crack-like planar defects, the following points are worth reiterating:

- The beam width of the given SH-wave EMAT is 9.46˚ as per Equation 5.1 and Equation 5.2. The tests carried out with the same EMAT on crack-like defects, results of which are presented in Figure 5.6; assess the inspection capability of the EMAT sensor from a distance of 2 feet, at three different lateral positions relative to the centerline of the crack. It can be concluded that for a limited distance d, the total inspection area would approximately cover a triangular region of area $0.166d^2$.

- Assuming a noise floor of around 5 mV, which is typical of the collected data shown in Figure 5.7, the maximum potential distance from which a 50% through-wall, 6 inch wide crack can be inspected using the SH0 mode from a single location, is around 13 feet in one direction. Thus the SH0 mode is extremely sensitive to crack-like defects.

- An experiment on the steel plate buried under a 3.5 inch thick concrete slab was conducted. Figure 5.10 shows that as the concrete stiffens the amplitude of the echo reflection from the crack drops. When the concrete was completely dry, the amplitude was found to have dropped to zero. This is an important observation which suggests that if the concrete is strictly bonded to the plate, the inspection

capabilities of the EMAT cannot be validated. However, it was found that if one tapped the concrete on the sides, the amplitude level comes up to a value of 20 mV. This tapping could have weakened the concrete-steel interface which is why the ultrasound energy was able to penetrate the structure. Case histories suggest that most concrete reinforced civil structures that require inspection have some amount of de-lamination because of differential thermal expansion. Thus the tapping can be approximated to such de-lamination and the inspection can be thus confirmed to be valid.

CHAPTER 6

FINITE-ELEMENT ANALYSIS OF PLATE-LIKE STRUCTURES

The ability to model and simulate guided wave propagation provides an insight into the development of robust guided wave inspection systems. This chapter presents the finite-element method (FEM), as a powerful computational technique used in the context of ultrasonic guided wave thickness estimation in inaccessible plate like structures.

[Krautkrämer and Krautkrämer 1990] illustrates the use of ultrasonic bulk waves for thickness estimation of plate structures by measuring time-of-flight. This method requires a point-by-point inspection of the entire region, thus increasing labor costs and inspection time. Ultrasonic guided waves provide an attractive alternative since they can travel over considerable amounts of distance and thus, apart from reducing inspection time and cost, can also be used to acquire information about regions that are otherwise difficult or impossible to access.

[Luo and Rose 2003] and [Luo and Rose 2004] used features like group velocity and frequency to estimate the thickness of uniform plates of different thicknesses using EMATs and piezoelectric transducers respectively. The object of this study is to develop a method to estimate average thickness in plate-like structures having small and gradual changes in their thickness profile using FEM as a tool.

6.1 Theoretical Construct

Guided waves can propagate within a plate only for specific combinations of frequency and phase velocity. For Lamb type waves, these combinations are given by the roots of the following Rayleigh-Lamb frequency relations.

$$\frac{\tan(qh)}{\tan(ph)} = -\frac{4k^2pq}{(q^2-k^2)^2} \qquad [6.1]$$

$$\frac{\tan(qh)}{\tan(ph)} = -\frac{(q^2-k^2)}{4k^2pq} \qquad [6.2]$$

Equation 6.1 corresponds to the family of symmetric modes while Equation 6.2 corresponds to the family of antisymmetric modes. p is given as per Equation 6.3 and q is defined as per Equation 6.4.

$$p = \sqrt{\frac{\omega^2}{c_L^2} - k^2} \qquad [6.3]$$

$$q = \sqrt{\frac{\omega^2}{c_T^2} - k^2} \qquad [6.4]$$

Here c_L is the longitudinal velocity, c_T is the shear velocity, k is the wave number, h is the plate thickness and ω is the frequency [Rose 1999]. From the Rayleigh-Lamb equations, it can be observed that if the thickness of the plate changes, frequency and velocity changes will be found too. For the purpose of this study, only group velocity has been analyzed to estimate average thickness in inaccessible plate-like structures.

6.2 The Finite-Element Method

A 2-D plane strain model of a 6.35 mm thick steel plate was developed using commercially available software, ABAQUS [ABAQUS 2007]. The explicit solver available within ABAQUS was employed to obtain wave propagation through the FEM model. The material properties for steel defined for the FEM model are given below in Table 6.1.

Table 6.1: Material properties defined in ABAQUS.

Density (kg/m^3)	Young's modulus (GPa)	Poisson's ratio
7800	200	0.3

As illustrated by Equation 6.5, for an isotropic material like steel, the longitudinal velocity c_L is a function of the Elastic modulus *E,* the material density ρ and Poisson's ratio ν while the shear velocity c_T is given by Equation 6.6.

$$c_L = \sqrt{\frac{E(1-\nu)}{\rho(1+\nu)(1-2\nu)}} \qquad [6.5]$$

$$c_L^2 = \frac{c_T^2(1-2\nu)}{2(1-\nu)} \qquad [6.6]$$

Equation 6.7 and Equation 6.8 show the longitudinal and shear velocities calculated using the material values of Table 6.1 in Equation 6.1 and Equation 6.2 respectively.

$$c_L = 5.875\ mm/\mu sec \qquad [6.7]$$

$$c_T = 3.14 \ \ mm / \mu sec \qquad [6.8]$$

The velocities calculated in Equation 6.7 and Equation 6.8 was used to generate dispersion curves for a 6.35 mm thick steel plate as shown in Figure 6.1. The low frequency dispersive region of the A0 mode at a frequency*thickness (*fd*) product equal to 0.7 MHz-mm was used in this analysis. This region was selected as it was expected to have good sensitivity to smooth thickness changes. Figure 6.1 illustrates this excitation region for a 6.35 mm thick steel plate.

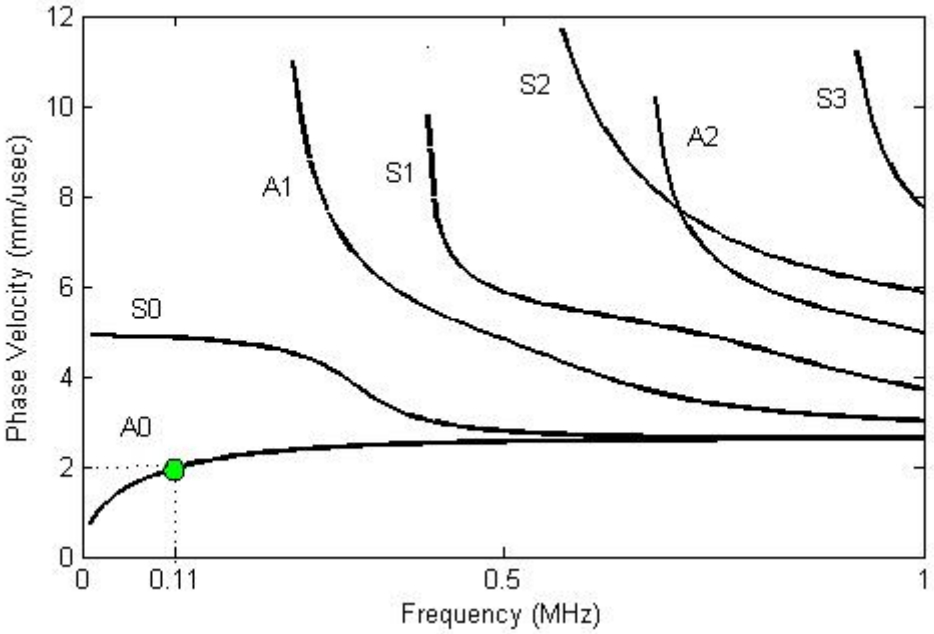

Figure 6.1: Lamb waves phase velocity dispersion curves for a 6.35 mm thick steel plate assuming a longitudinal bulk velocity of 5.875 mm/µsec and a shear bulk velocity of 3.14 mm/µsec. The A0 mode is shown to be excited at 110 kHz.

A 7-cycle Hanning-windowed toneburst centered at 110 kHz was used as the excitation signal as shown in Figure 6.2. Figure 6.3 illustrates the FEM model of an undamaged steel plate. The receiving sensor was set 50 inches away from the transmitter

and was used to record the arriving wave packet as it propagated through the steel plate model.

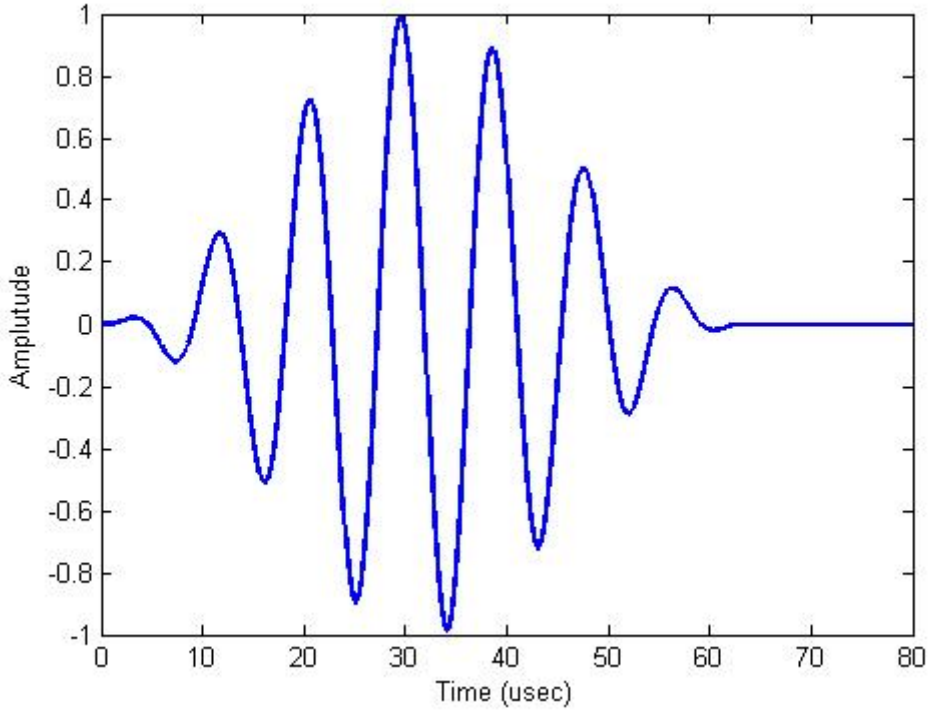

Figure 6.2: A 7-cycle Hanning-windowed 110 kHz toneburst signal used for A0 mode generation in the finite-element models.

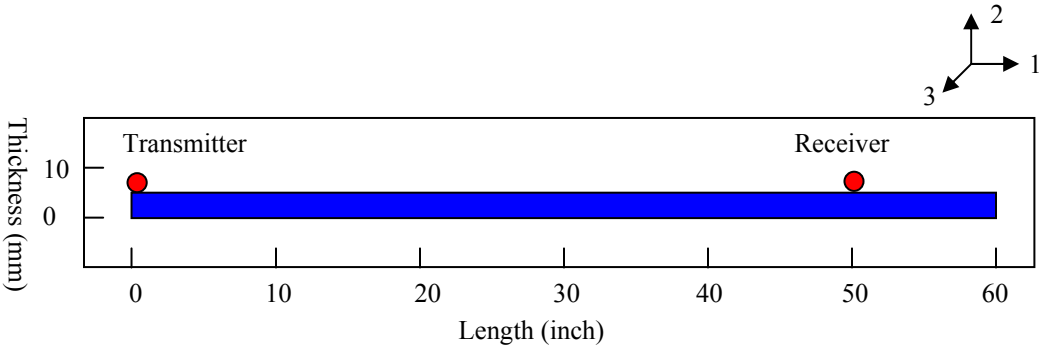

Figure 6.3: The FEM model of an undamaged steel plate. Plate is 60 inches long and 6.35 mm thick. Transmitter is at left edge of plate and receiver is 50 inches further away.

Figure 6.4 provides the wave structure of the mode at the given excitation region. Two sets of eleven points each, which define the in-plane (U_1) and out-of-plane (U_2) displacement, were used as loading conditions along the left edge of the plate to generate a pure A0 mode.

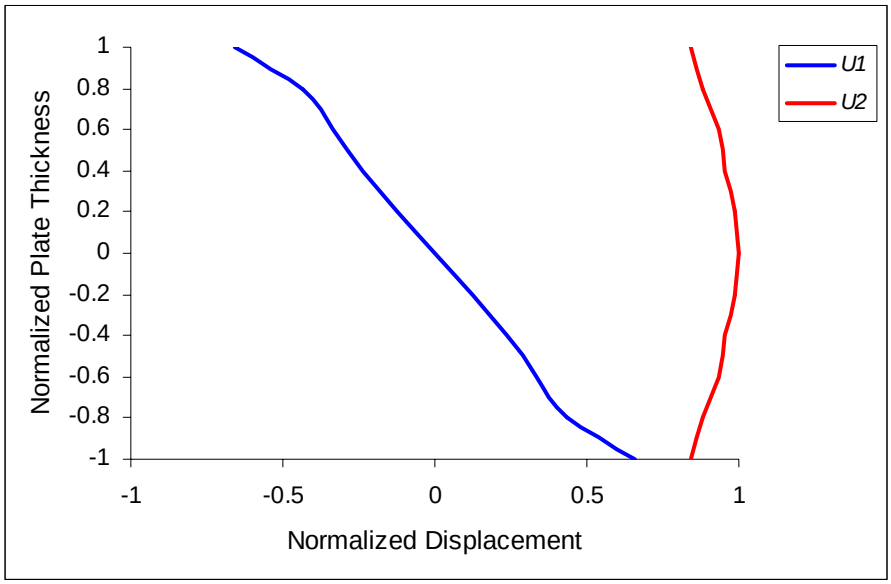

Figure 6.4: Wave structure of the A0 mode in a 6.35 mm thick steel plate at 110 kHz, showing the in-plane (blue line) and out-of-plane (red line) displacement components along the plate thickness.

Figure 6.5 shows the theoretical group velocity trend of the A0 mode excited at a frequency of 110 kHz for a 6.35 mm thick steel plate. The velocity drops from 3.05 mm/µsec to 2.7 mm/µsec as the thickness of the plate reduces to 50 % of original plate thickness.

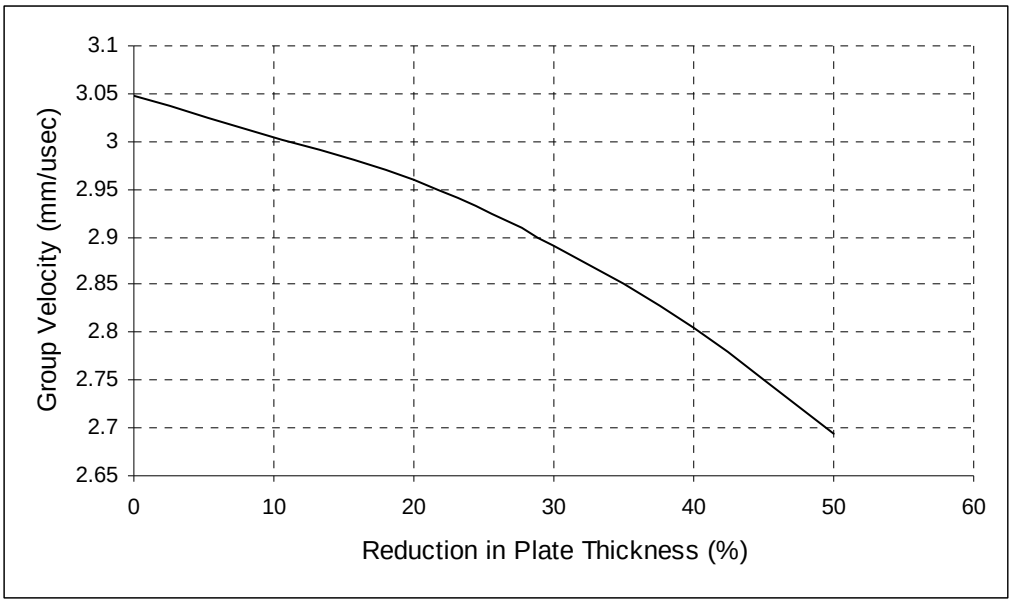

Figure 6.5: Theoretical group velocity trend for the A0 mode excited at a frequency of 110 kHz. The original plate thickness is 6.35 mm. It is observed that the group velocity drops from 3.05 mm/μsec to 2.7 mm/μsec as the thickness of the plate was reduced to 50 % of original plate thickness.

6.2.1 Model Accuracy

Before proceeding with complex modeling, it is essential to check the accuracy of the FEM model. This can be done by comparing theoretically known features like wave structure and group velocity with the FEM calculated results [Luo 2005].

As observed from Figure 6.4, the A0 mode has a dominant out-of-plane displacement throughout the plate thickness for the given excitation region. Figure 6.6 (a) and (b) respectively show the ABAQUS in-plane and out-of-plane displacement outputs extracted at the receiver node. Comparing (a) and (b), it can be seen that the modeling results are consistent with the theoretical results.

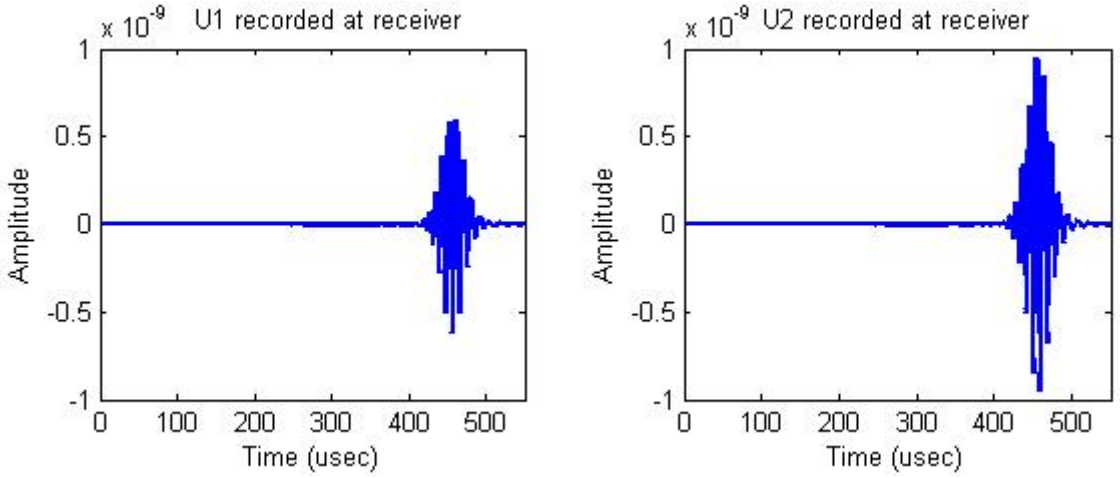

(a) (b)

Figure 6.6: ABAQUS output of displacement at the receiver node – (a) U_1 component, (b) U_2 component.

Figure 6.7 displays the transmitted and received A0 mode excited at a frequency of 110 kHz on a 6.35 mm thick and 60 inch long steel plate model. The ultrasonic guided wave was launched from the extreme left edge of the plate and was allowed to propagate over a distance of 50 inches before being received at the receiving node. Total travel time of the wave is calculated to be approximately 425 µseconds, thus giving a group velocity measurement of 2.987 mm/µsec. The theoretical group velocity as per Figure 6.5 is 3.05 mm/µsec. Thus the FEM error is around 2%, which is totally acceptable.

As a final validation, four more ABAQUS/Explicit models were created having uniform thicknesses reductions of 20-50 % of the original 6.35 mm thick FEM model shown in Figure 6.3. For each of these models, group velocity measurements were made similar to that shown in Figure 6.7. These results along with the theoretical values of group velocity for reducing plate thicknesses are shown in Figure 6.8.

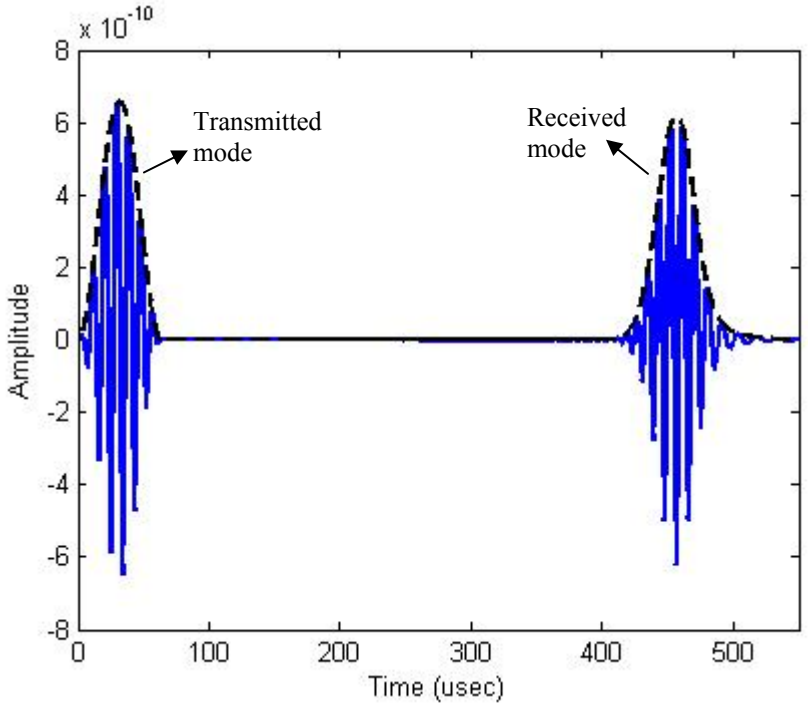

Figure 6.7: FEM group velocity measurement for a 6.35 mm thick steel plate. The A0 wave was transmitted from the left edge of the plate model and was allowed to propagate a distance of 50 inches before being received. The black dotted line is the analytic envelope of the waveform. The measured group velocity thus works out to be 2.987 mm/µsec. Theoretical group velocity = 3.05 mm/µsec.

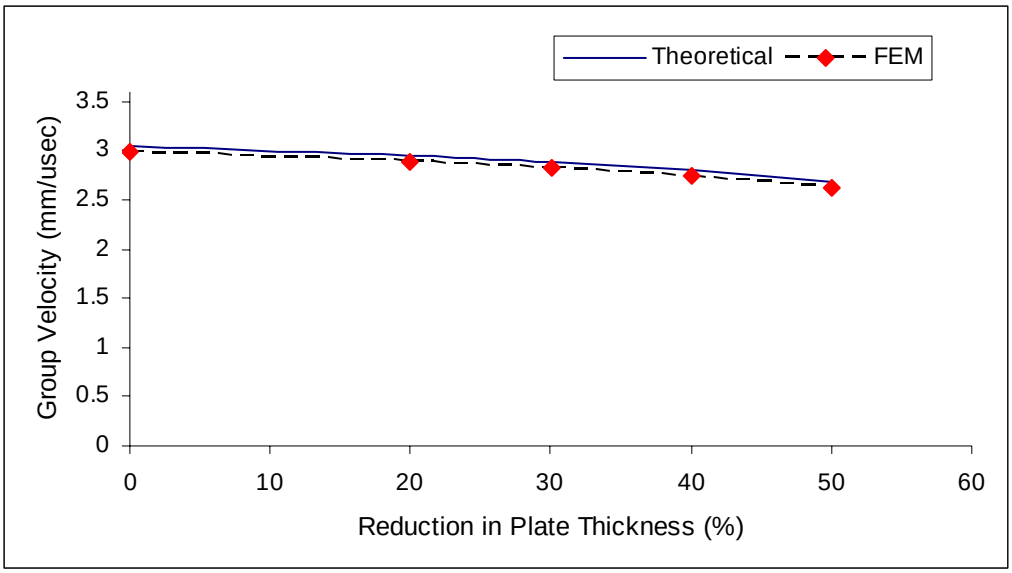

Figure 6.8: Plot of theoretical values (black line) and FEM calculated values (red diamonds) of the group velocity of the A0 mode at 110 kHz for reducing plate thicknesses.

6.2.2 A Parametric Study on Non-Uniform Plate Thinning

The validations of the previous sub-section have laid a strong foundation for the work presented in this sub-section of the chapter, which explores the effect of small and gradual changes in the thickness profile of a plate on group velocity.

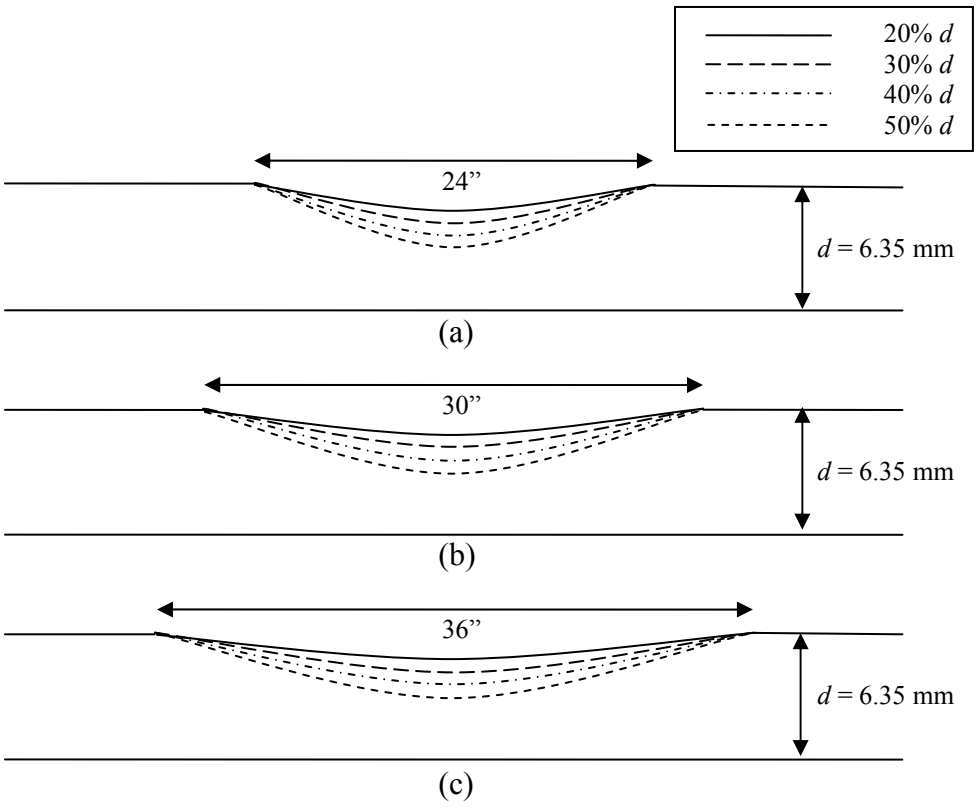

Figure 6.9: Thinning specimens modeled for the parametric study on group velocity shifting – (a) Thinning length of 24”, (b) Thinning length of 30”, (c) Thinning length of 36”. Damaged section was modeled in ABAQUS using 3 points on an arc corresponding to the start of damage, end of damage and maximum depth of damage.

A parametric study was carried out, where the depth of damage was varied for three different lengths of damage as shown in Figure 6.9 (a), (b) and (c). An elliptical shaped damage was considered for purposes of the analysis. A through transmission

mode was employed similar to the previous sub-section with the transmitter on the left edge of the plate and the receiver 50 inches away on the other side of the damage.

Figure 6.10 (a), (b) and (c) display the received A0 mode for the three different damage lengths corresponding to Figure 6.9 (a), (b) and (c) respectively. A few noteworthy observations can be made from the illustrations. In Figure 6.9 (a), for damage length of 24" and a minimum damage depth of 50% the original plate thickness (pink envelope), the A0 mode is observed to have arrived at 474 μseconds. In Figure 6.9 (c), for damage length of 36" and a minimum damage depth of 40% the original plate thickness (blue envelope), the A0 mode is observed to have arrived at 474 μseconds.

Based on these observations, an interesting conclusion can be drawn. Apart from damage depths affecting the group velocity of the propagating A0 mode thus affecting its arrival time, the length of the damage also plays a role in delaying the mode. Thus the time taken for the mode to reach its destination is a function of two unknowns, the damage depth and the damage length.

Figure 6.11 condenses the waveforms of Figure 6.9 (a), (b) and (c) into one single plot which also shows the theoretical group velocities for a uniform plate of varying thicknesses as a thick black line. This figure thus ratifies the intuitive notion that if the length of the elliptical damage is increased further, the depth will spread out over a larger cross-section of this ellipse and the plate will look more like a uniformly thinner plate, thus approaching the theoretical bound.

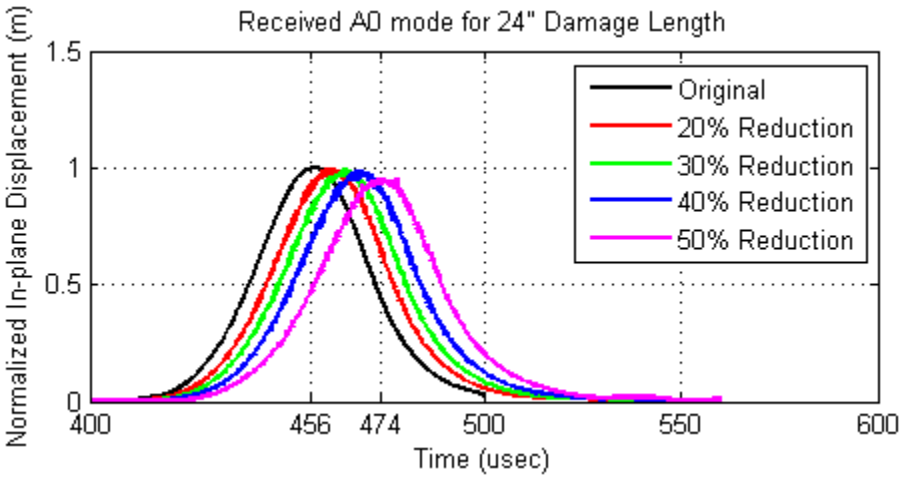

(a)

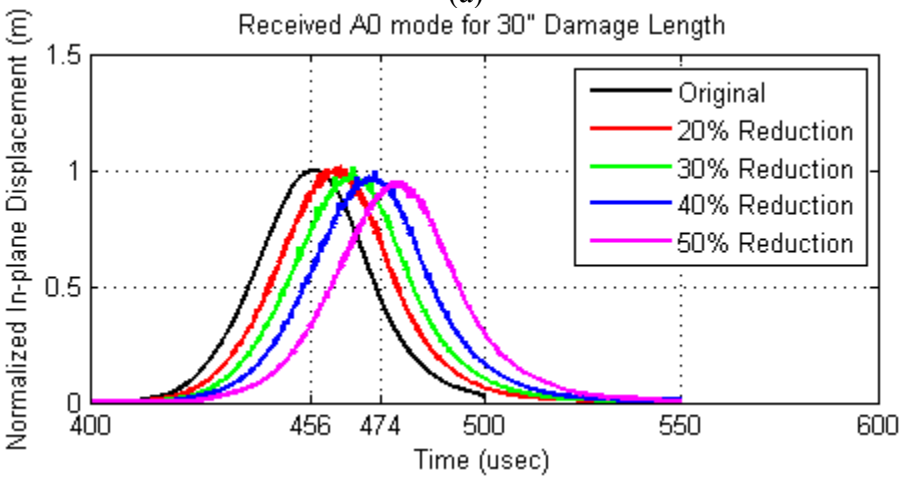

(b)

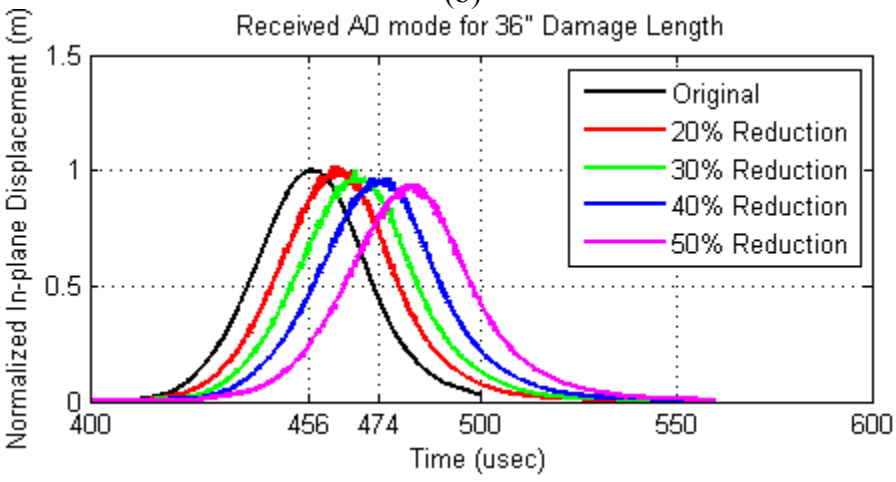

(c)

Figure 6.10: Analytic envelopes of the A0 mode at 110 kHz for different damage depths recorded at the receiver node for – (a) 24” length damage, (b) 30” length damage and (c) 36” length damage.

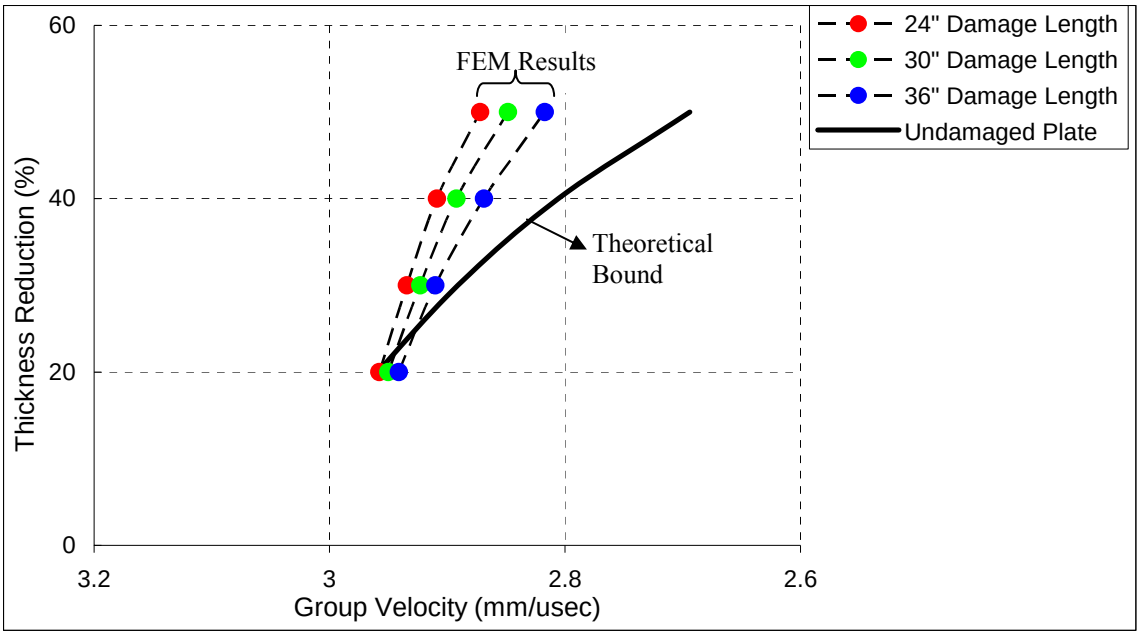

Figure 6.11: FEM calculated group velocities of the A0 mode for all combinations of damage length and depths. The thick black line is the theoretical bound obtained from Fig 5.5. Based on these curves, it can be concluded that damage depth as well as length have an impact on the arrival times of the wave packet.

6.2.3 Estimate of Average Plate Thickness

Using the FEM models of the previous sub-section, the average thickness of the plate, t_{avg} between the two sensors, is calculated using Equation 6.9. The dimensions correspond to the cross-section of the plate between the two sensors shown in Figure 6.12. All the calculated results are tabulated in Table 6.2 along with the FEM calculated group velocities.

$$t_{avg} = \frac{(l_1 d) + (l_2 d) + \left[(2ad) - \left(\frac{\pi ab}{2} \right) \right]}{l} \qquad [6.9]$$

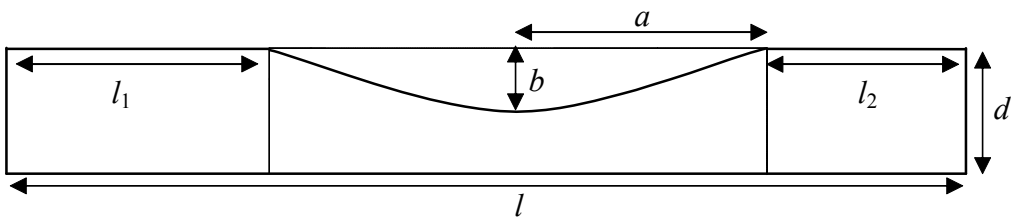

Figure 6.12: Dimensions used to calculate average thickness of structure being evaluated.

Table 6.2: Mathematically calculated average thickness and FEM calculated group velocities.

Length (inch) / Depth (%)	24		30		36	
	Avg. Thickness (mm)	Grp. Velocity (mm/μsec)	Avg. Thickness (mm)	Grp. Velocity (mm/μsec)	Avg. Thickness (mm)	Grp. Velocity (mm/μsec)
20	5.87	2.96	5.75	2.95	5.63	2.94
30	5.63	2.93	5.45	2.92	5.27	2.91
40	5.39	2.91	5.15	2.89	4.91	2.87
50	5.15	2.87	4.85	2.84	4.55	2.82

Figure 6.13 shows a plot of average thickness loss between the two sensors and the FEM calculated group velocities of the A0 mode. Since a total of twelve computer runs were made for different combinations of damage depths and lengths, there are twelve data points in the plot. For the sake of visibility, the data point corresponding to an undamaged plate model is also shown corresponding to a 0% average thickness loss.

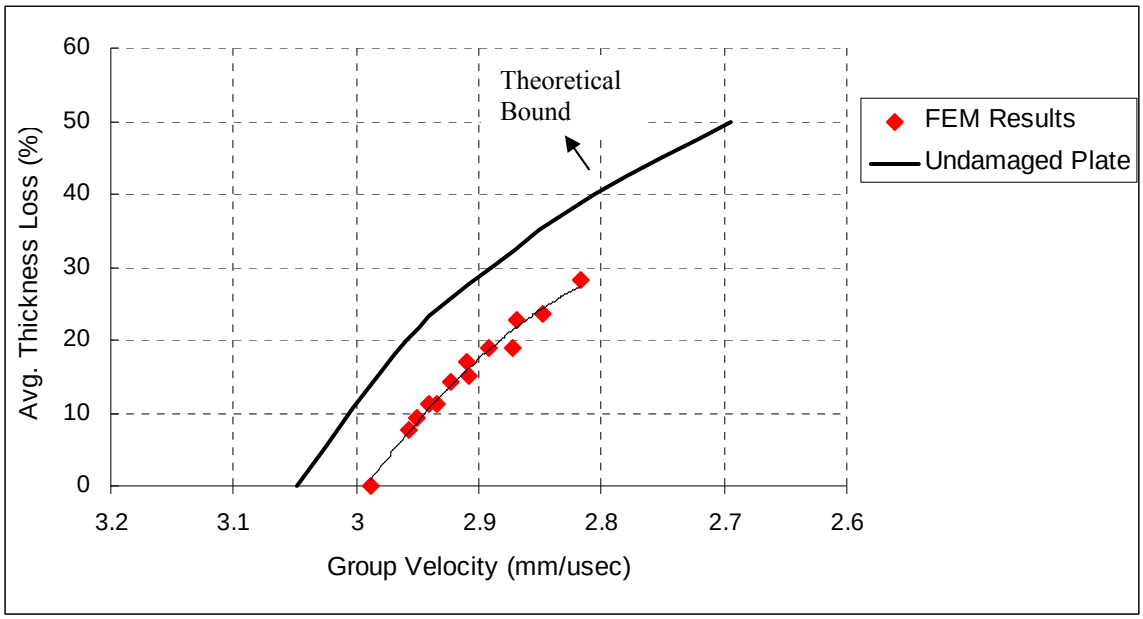

Figure 6.13: Plot of 'Average Thickness Loss' versus 'FEM calculated Group Velocities' of the A0 mode.

6.3 Discussion and Summary

In this chapter, a guided wave finite element analysis of a steel plate having gradual thickness changes was conducted. Validations on the accuracy of the basic FEM model were carried out before proceeding with a parametric study on non-uniform plate thinning. An elliptical shaped damage was selected for this purpose and the group velocity of the A0 mode at a *fd* product equal to 0.7 MHz-mm was used as a feature. It was found that both damage depth as well as damage length have an effect on the wave mode traveling through the damage.

The average thickness of the plate was calculated for different combinations of damage length and depth and an attempt to correlate average thickness loss with group velocity changes was made. Figure 6.13 shows that the trend followed by the group velocities of the A0 mode in a plate having non-uniform thickness changes (dashed line) is similar to that followed by group velocities in a uniform thickness plate (thick black line). This phenomenon has significant import, since group velocity can be used as a measure to solve the inverse problem of estimating average thickness of a plate between two sensors. The theoretical group velocity then remains as an upper bound and the average thickness loss in a plate can never be more than that suggested by this limiting bound.

CHAPTER 7

SUMMARY AND FUTURE DIRECTION

7.1 Summary

A concise introduction and the objective behind this work were presented in Chapter 1. Chapter 2 provided a review of previous works that proved as a reference for this work. Chapter 3 highlighted the problem and statement of work. Figure 3.1 provides an example where the work presented here could be put to use. Photographs of the prototype model used for the analysis are provided in Figure 3.2 (a) and (b). The guided wave method has been proposed in this chapter too.

Chapter 4 laid emphasis on choosing the appropriate transducer based on penetration power studies for both Lamb wave and Shear Horizontal waves. Table 4.1 and Table 4.2 summarize the results of these studies. It was found that the fundamental mode of the SH-wave family showed very little energy leakage to the sand-water mix. Figure 4.6 suggests that the potential inspection distance attainable with the SH0 mode is more than 6 feet.

Chapter 5 delves into the beam spreading phenomenon of an Electromagnetic Acoustic Transducer (EMAT) used for generating SH waves. Equation 5.1 and Equation

5.2 suggest that the beam width of the EMAT used is approximately 9.46˚. Sensitivity of the SH0 wave to planar defects was also studied in this chapter. For this a 6 inch wide crack-like defect was fabricated on a 3/8 inch thick steel plate as shown in Figure 5.5 (a). By *rastering* the EMATs in a pitch-catch arrangement along the width of the plate, the beam width was verified to be close to 9˚. A penetration power study on the crack-like defect was conducted. Figure 5.6 suggests that the SH0 wave can potentially inspect for planar defects up to 13 feet in one direction from a single location. An experiment with the plate buried under concrete was also performed. Figure 5.10 shows that as the concrete stiffened the amplitude of the echo reflection from the crack dropped.

Chapter 6 proposes a hybrid analytic FEM wave propagation technique to inspect for gradual corrosion-type thinning in plates. For this the low frequency dispersive region of the A0 mode was used and group velocity changes were measured to estimate the average thickness loss of the plate between a transmitter and a receiver. Table 6.2 summarizes the results of this study and Figure 6.13 provides an FEM proposed curve to solve the inverse problem of quantifying average thickness loss.

7.2 Future Direction

A framework for the development of an ultrasonic guided wave inspection system for hard to access civil structures has been laid down. Using the fundamental SH wave mode in a pulse echo mode, one can inspect cracks which are not necessarily in line with

the sensor. For small gradual thinning changes, a through transmission mode can be used to inspect between two random points of the structure.

However, quoting the ancient Greek philosopher Epicurus, "*Nothing is enough for the man to whom enough is too little*", the following areas of future research and development are proposed:

- This study looked at wet sand and cement as possible barriers against gaining access to the plate-like structure. The interrogation of other possible hindrances needs to be carried out too.

- Sensitivity of planar crack-like defects was analyzed using the fundamental mode of the SH-wave family. Other defect geometries and formations need to be investigated.

- The hybrid analytic FEM technique used in this study focused on elliptical like damage only. A more irregular shaped damage would be an interesting case for further study. The FEM modeling was done on 2D corrosion type damage for Lamb waves. Shear wave propagation modeling requires 3D modeling because of its loading constraint. Modeling defects in 3D would be a challenging task but the results of the analysis could prove to be enriching.

- Integration of experimentally driven analysis of wave propagation with real-time data acquisition and data processing systems would enable such an inspection system to be aptly used for the thorough non-destructive evaluation of hard to access civil structures.

BIBLIOGRAPHY

Abaqus, Inc. (2007) *ABAQUS/CAE v6.7* [Computer Software]. Pawtucket, RI: ABAQUS, Inc. 2007.

Achenbach, J. D., *"Quantitative Nondestructive Evaluation"*, International Journal of Solids and Structures, vol. 37, no. 1-2, pp. 13-27, 2000.

Breon, L. J., "*Ultrasonic Guided Wave Thickness Measurement Of Isotropic Plate-like Structures"* (M.S. Thesis), The Pennsylvania State University, 2008.

Cawley, P., Alleyne, D., "*The use of Lamb waves for the long range inspection of large structures*", Ultrasonics, vol. 34, no. 2-5, pp. 287-290, 1996.

Fortunko, C. M., King, R. B., *et al*., *"Nondestructive Evaluation of Planar Defects in Plates using Low-Frequency Shear Horizontal Waves"*, Journal of Applied Physics, vol. 53, pp. 3450-3458, 1982.

Graff, K. F., "*Wave Motion in Elastic Solids*", Ohio State University Press, 1975.

Hirao, M., Ogi, H., *"EMATS for Science and Industry Noncontacting Ultrasonic Measurements"*, Kluwer Academic Publishers, 2003.

Jenot, F.,Ouaftouh, M., *et al,* "*Corrosion thickness gauging in plates using Lamb wave group velocity measurements*", Measurement Science and Technology, vol. 12, pp. 1287-1293, 2001.

Jenot, F., Ouaftouh, M, "*Finite Element Modeling of Guided Waves Propagation in Plates with Variable Thickness",* Proceedings of the International Congress on Ultrasonics. Vienna, 2007.

Krautkrämer, J., Krautkrämer, H., Ultrasonic Testing of Materials, New York: Springer Verlag, 1990

Luo, W., "*Ultrasonic Guided Waves and Wave Scattering in Viscoelastic Coated Hollow Cylinders"* (Ph.D. Thesis), Engineering Science and Mechanics, The Pennsylvania State University, 2005.

Luo, W., Rose, J. L., "*Guided wave thickness measurement with EMATs"*, Insight, vol. 45, no. 11, pp. 735-739, 2003.

Luo, W., Rose, J. L., "*Lamb wave Thickness Measurement Potential with Angle Beam and Normal Beam Excitation",* Materials Evaluation, vol. 62, no. 8, pp. 860-866, 2004.

Mirkhani, K., *et al*., *"Optimal Design of EMAT Transmitters",* NDT & E International, vol. 37, pp. 181-193, 2004.

Pavlakovic, B. N., Lowe, M. J. S., Cawley, P., *"High-Frequency Low-Loss Ultrasonic Modes in Imbedded Bars"*, Journal of Applied Mechanics, vol. 68, pp. 67-75, 2001.

Rose, J. L., Ditri, J. J., *et al*., *"A Guided Wave Inspection Technique for Nuclear Steam Generator Tubing"*, NDT & E International, vol. 27, no. 6, pp. 307-310, 1994.

Rose, J. L. "*Ultrasonic Waves in Solid Media",* Cambridge University Press, 1999.

Rose, J. L., *"Guided Wave Nuances for Ultrasonic Nondestructive Evaluation"*, IEEE Transactions on Ultrasonics, FerroElectrics, and Frequency Control, vol. 47, no. 3, pp. 575-583, 2000.

Rose, J. L., *"A Baseline and Vision of Ultrasonic Guided Wave Inspection Potential",* Journal of Pressure Vessel Technology, vol. 124, no. 3, pp. 273-282, 2002.

Rose, J. L., *"Guided Wave Testing of Water Loaded Structures*", Materials Evaluation, vol. 61, pp. 23-24, 2003.

Silk, M. G., *"Ultrasonic Transducers for Nondestructive Testing*", Adam Hilger Ltd, Bristol, 1984.

Vasile, C. F., Thompson, R. B., *"Periodic Magnet Non-Contact Electromagnetic Acoustic Wave Transducer-Theory and Application*" Proceedings 1977 IEEE Ultrasonics Symposium, pp. 84-88, 1977.

Wilcox, P. D., Lowe, M. S. J., Cawley, P., *"The Effect of Dispersion on Long-range Inspection using Ultrasonic Guided Waves"*, NDT & E International, vol. 34, no. 1, pp. 1-9, 2001.

Zhao, X. *"Quantitative Defect Characterization via Guided Waves*", (Ph.D. Thesis), Engineering Science and Mechanics, The Pennsylvania State University, 2003.

Zhu, W., Rose, J. L., Barshinger, J. N., Agarwala, V. S., *"Ultrasonic Guided Wave NDT for Hidden Corrosion Detection*", Research in Nondestructive Evaluation, vol. 10, no. 4, pp. 205-225, 1998.